REVIEW ARTICLE

Check for updates

Bioapplications of DNA nanotechnology at the solid–liquid interface

Wenjing Wang, [ab] Sha Yu, [a] Shan Huang, [a] Sai Bi, [c] Heyou Han, *[b]
Jian-Rong Zhang, *[a] Yi Lu [d] and Jun-Jie Zhu *[a]

DNA nanotechnology engineered at the solid–liquid interface has advanced our fundamental understanding of DNA hybridization kinetics and facilitated the design of improved biosensing, bioimaging and therapeutic platforms. Three research branches of DNA nanotechnology exist: (i) structural DNA nanotechnology for the construction of various nanoscale patterns; (ii) dynamic DNA nanotechnology for the operation of nanodevices; and (iii) functional DNA nanotechnology for the exploration of new DNA functions. Although the initial stages of DNA nanotechnology research began in aqueous solution, current research efforts have shifted to solid–liquid interfaces. Based on shape and component features, these interfaces can be classified as flat interfaces, nanoparticle interfaces, and soft interfaces of DNA origami and cell membranes. This review briefly discusses the development of DNA nanotechnology. We then highlight the important roles of structural DNA nanotechnology in tailoring the properties of flat interfaces and modifications of nanoparticle interfaces, and extensively review their successful bioapplications. In addition, engineering advances in DNA nanodevices at interfaces for improved biosensing both in vitro and in vivo are presented. The use of DNA nanotechnology as a tool to engineer cell membranes to reveal protein levels and cell behavior is also discussed. Finally, we present challenges and an outlook for this emerging field.

[a] State Key Laboratory of Analytical Chemistry for Life Science, School of Chemistry & Chemical Engineering, Nanjing University, Nanjing 210023, China.
E-mail: jjzhu@nju.edu.cn, jrzhang@nju.edu.cn

[b] State Key Laboratory of Agricultural Microbiology, College of Science, Huazhong Agricultural University, Wuhan 430070, China.
E-mail: hyhan@mail.hzau.edu.cn

[c] College of Chemistry and Chemical Engineering, Qingdao University, Qingdao 266071, China

[d] Department of Chemistry, University of Illinois at Urbana-Champaign, Urbana 61801, USA

1. Introduction

DNA, the blueprint of life, is a structurally simple, yet a functionally complex molecule that has been used to engineer new nanotechnologies.[1] DNA nanotechnology began in the 1980s by using DNA as a building block to construct nanoscale patterns, and has now grown to include a wide range of research fields. Over the last few decades, DNA nanotechnology has rapidly developed from solely structural DNA nanotechnology to include dynamic and functional DNA nanotechnology.

Initial research focused on constructing exquisite nanopatterns, manipulating dynamic DNA behavior and selecting new types of functional DNA molecules. The establishment of new principles has inspired researchers to pursue practical bioapplications.[2–6] In an effort to develop more advanced

bioapplications, DNA nanotechnology has moved from solely aqueous solutions to solid–liquid interfaces. The facile modification feature of DNA has facilitated the engineering of interfaces based on different principles. The most widely used method is thiol-gold chemistry. Spherical nucleic acid (SNA), wherein thiolated DNA is conjugated to gold nanoparticles, is a well-known example that was demonstrated by Mirkin.[7] A potential problem with this engineering approach is that DNA can be replaced from gold nanoparticles by more reductive molecules in cells and tissues (e.g., glutathione), thereby hampering in vivo bioapplications.[8] Since DNA is negatively charged because of the phosphate backbone, electrostatic interaction is another commonly used strategy to attach DNA molecules to positively charged surfaces.[9] Potential drawbacks of this method are limited stability and integrity, which can lead to nonspecific release of the attached DNA molecules by other charged species during applications. New interfaces involving DNA molecules have been developed using other covalent and noncovalent approaches, including biotin–streptavidin interaction[10] and click chemistry.[11] We have listed only the most widely used approaches above; given the broad range of DNA nanotechnology, other approaches involving a variety of interfaces will be discussed in extensive detail throughout the review.

Based on shape and component features, solid–liquid interfaces can be divided into three main categories: flat interfaces,

Left to right: Sha Yu, Wenjing Wang and Shan Huang

Sha Yu (Left) is now a PhD candidate majoring in Analytical Chemistry at the School of Chemistry and Chemical Engineering of Nanjing University. She received her BS from the College of Chemistry & Materials Science of Northwest University in 2015. Her current research interests focus on the assembly of DNA nanostructures and their applications in biosensing, bioimaging and targeted cancer therapy. Wenjing Wang (Middle) received her BS degree from Northwest University in 2011 and PhD degree from Nanjing University in 2017 under Professor Jian-Rong Zhang and Professor Jun-Jie Zhu. She is currently an associate professor in the College of Science of Huazhong Agricultural University. Her research interests include DNA nanotechnology-based biosensing and bioimaging of intracellular cancer biomarkers. Shan Huang (Right) received her BS degree in 2014 from the Harbin University of Commerce, China, and MSc degree in 2017 from Ningxia Medical University, China. She is a PhD candidate majoring in analytical chemistry under the supervision of Prof. Jian-Rong Zhang and Prof. Jun-Jie Zhu in Nanjing University. Her research interests focus on the detection of intracellular functional molecules using DNA nanotechnology.

Sai Bi

Sai Bi received her PhD degree from Qingdao University of Science and Technology in 2010. She worked as a postdoctoral fellow at Nanjing University from 2012 to 2014. She is currently a professor in College of Chemistry and Chemical Engineering at Qingdao University. Her research interests focus on biochemical analysis, DNA nanotechnology, molecular imaging and targeting therapy.

Heyou Han

Heyou Han received his PhD in analytical chemistry from the Wuhan University in 2000. From 2000 to 2002, he was a postdoctoral researcher at the University of Science and Technology of China. Currently, he is a professor in the State Key Laboratory of Agricultural Microbiology, College of Science from Huazhong Agricultural University (China). He also serves as the Executive Vice Dean of the Graduate School in Huazhong Agricultural University. His research mainly focuses on developing new analysis methods to detect pathogenic microorganisms including virus and bacteria in agriculture.

Jian-Rong Zhang

Jian-Rong Zhang was born in 1963 in Wujiang City of Jiangsu Province. He received BSc (1984), MSc (1987), and PhD (1990) from Nanjing University. After obtaining his PhD degree, he worked at Nanjing University as a Lecturer in 1990 and a Professor in 2003. His research interests include the synthesis of novel functionalized nanomaterials and fabrication of self-powered biosensors. He has published more than 150 papers and received a number of national and ministerial awards.

Yi Lu

Dr Yi Lu received his BS degree from Peking University in 1986 and a PhD degree from UCLA in 1992. After two years of postdoctoral research in Professor Harry B. Gray's group at Caltech, he started his independent career at UIUC, in 1994. He is now a Jay and Ann Schenck Professor of Chemistry in the Departments of Chemistry, Biochemistry, Bioengineering and Materials Science and Engineering. His research interests include bioinorganic, biomaterials and bioanalytical chemistry, and their application as catalysts in renewable energy generation and pharmaceuticals, and as sensors and agents in environmental monitoring, medical diagnostics, imaging and targeted drug delivery.

nanoparticle interfaces and "soft" interfaces. Interfaces that serve as platforms for DNA immobilization and hybridization and as carriers have advanced our ability to manipulate the static and dynamic behavior of DNA for fundamental research and real-world applications. Interfaces with various shapes, sizes and constituents always exhibit distinct functions and properties; therefore, the integration of interfaces with DNA nanotechnology will provide unlimited possibilities for wider bioapplications. Flat interfaces engineered with structural DNA nanotechnology contribute to well-controlled, highly ordered biosensing platforms. Nanoparticle interfaces engineered with dynamic and functional DNA nanotechnology lead to spatiotemporal biosensing and bioimaging systems, activatable host-molecule release models and on-particle DNA nanodevices. These advances have paved the way for the development of new bioapplications in biosensing, bioimaging and biomedicine, providing effective tools and strategies for analytical, biomedical and related studies with unprecedented speed.

In this review, we summarize the numerous possibilities enabled by the integration of DNA nanotechnology with solid–liquid interfaces. Specifically, we briefly describe the development of DNA nanotechnology, and then comprehensively describe recent reports on the bioapplications of DNA nanotechnology at the solid–liquid interface which comprises flat interfaces, nanoparticle interfaces, and soft interfaces of DNA origami and cell membranes. Finally, we provide our perspectives and describe future challenges of this field in moving from laboratory investigations to practical applications.

2. DNA nanotechnology

The unceasing development of DNA nanotechnology has laid the foundation for advanced bioapplications. To better illustrate the most recent and inspiring bioapplications of DNA nanotechnology at solid–liquid interfaces, we begin with a brief overview of the development trajectory and recent advances in DNA nanotechnology. In contrast to the other reviews discussing DNA nanotechnology, we focus mainly on topics related to our

Jun-Jie Zhu is a Professor of Chemistry at Nanjing University, China. He received his BS (1984) and PhD (1993) degrees in Chemistry from Nanjing University. After this, he started his academic career at Nanjing University in 1993. During 1998–1999, he was a postdoctoral fellow in Bar-Ilan University, Israel. He mainly works in bioanalytical chemistry, including DNA nanotechnology based electrochemical and fluorescence biosensors and drug delivery.

Jun-Jie Zhu

He is also interested in the synthesis of biofunctional nanoparticles, and biological and biomedical applications of nanoparticles.

subsequent content. More details regarding the fundamentals of DNA nanotechnology can be found in other literature reports.[12–16]

2.1 Structural DNA nanotechnology

In addition to functioning as genetic material, DNA can be used as a building block to construct nanoscale patterns which is widely known as structural DNA nanotechnology. This research field was pioneered by Ned Seeman based on the unique Watson–Crick interaction of the nucleic acid base adenine and thymine (A–T), and cytosine and guanine (C–G).[17] Structural DNA nanotechnology employs DNA as a construction material to assemble complex shapes, including basic DNA nanostructures (Fig. 1A), 2D nanoscale patterns (Fig. 1B) and 3D nanostructures (Fig. 1C).[18–23] Using software,[24] it is possible even for nonspecialists from other disciplines to design and predict any shape. There are now routine design rules and assembly methods to engineer DNA nanostructures suited to different applications.[25]

Initially, branched DNA nanostructures were constructed using a sticky-end protocol by Ned Seeman. His vision was to create self-associating crystals with macromolecular-scale guests in a DNA host lattice.[26] As the branched structures were flexible and did not efficiently form more complex nanostructures, double-crossover (DX) and triple-crossover (TX) molecules were developed subsequently to circumvent the aforementioned drawbacks.[27,28] With these crossover motifs available, a series of advanced nanostructures have been constructed, including nanotubes, polyhedra, 2D/3D lattices and 3D crystals.[29–31]

Among all the complex constructions, tetrahedral DNA is a simple yet widely studied nanostructure[32] (Fig. 1D). Typically, tetrahedral DNA is composed of four oligonucleotide sequences that hybridize in a one-pot annealing reaction. A strand is designed to fold and hybridize with the other three strands to form one face of the tetrahedron, whose 5′ end meets the 3′ end at one edge. The vertex is left unpaired with "hinge" bases to accommodate the corresponding angle between adjacent edges. Each face consists of a rigid triangle of DNA helices, endowing the nanostructure with robust mechanical properties. Moreover, programming the four vertexes and six edges is rather straightforward. Thus, the integration of this elegant structure with other technologies has drawn attention from multidisciplinary research fields recently.[33–35]

DNA origami proposed by Paul Rothemund is another breakthrough in structural DNA nanotechnology.[36] A long single-stranded DNA (ssDNA) scaffold folds into a 3D lattice in a single step with the help of many short single staple strands (Fig. 1E). The process is extraordinarily precise and gives high yields. The staple strands can be modified to further attach functionalities including enzymes[37] and nanoparticles.[38] During the last decade, DNA origami has extended from 2D patterns to 3D nanostructures, and assemblies of 3D structures may contribute to the construction of devices with advanced functions.[39] Interestingly, a ssDNA or ssRNA was employed to construct 3D nanopatterns without the addition of any auxiliary strands.[40] The use of well-defined and addressable "soft" DNA origami nanostructures as interfaces should enable accurate
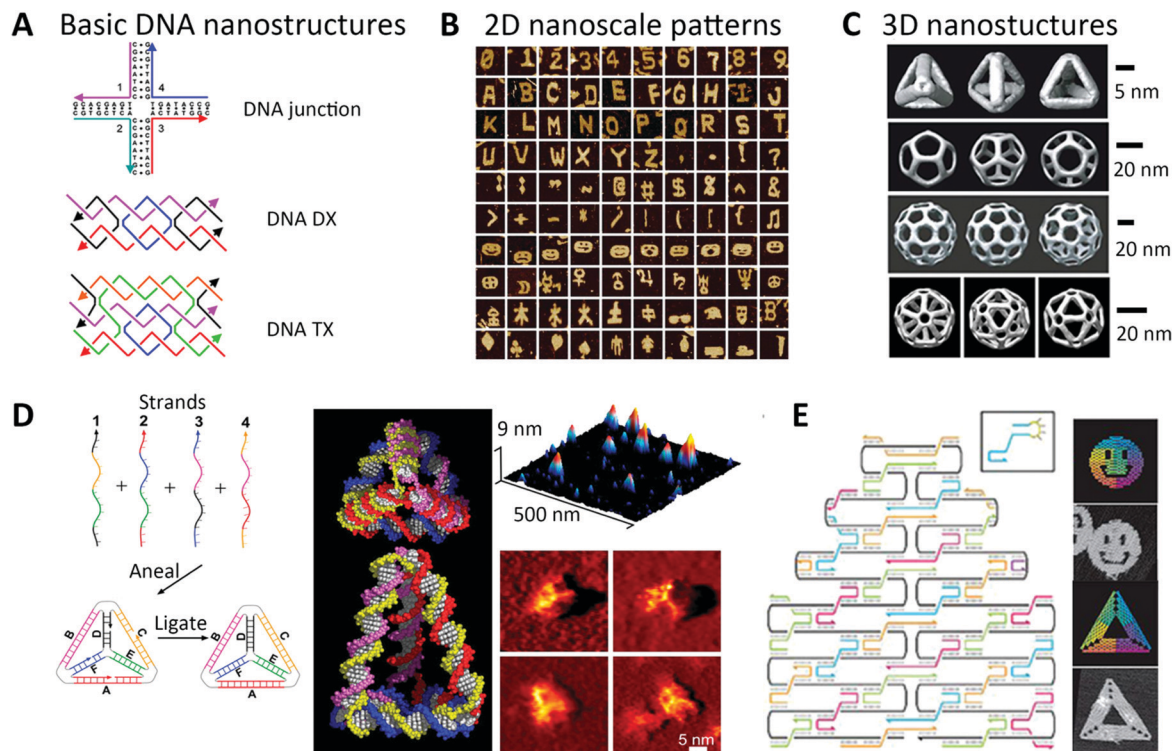
Fig. 1 (A) Basic DNA nanostructures used for the self-assembly of complex shapes, including four-way DNA junctions and DNA double-crossover (DX) and triple-crossover (TX) structures. Reprinted with permission from ref. 18. Copyright (2004) PLoS Biology. (B) Representative 2D nanoscale patterns. Reprinted with permission from ref. 21. Copyright (2012) Nature Publishing Group. (C) 3D nanostructures formed using DNA molecules as building blocks. Reprinted with permission from ref. 22 and 23. Copyright (2008) Nature Publishing Group (the first three rows). Copyright 2008 National Academy of Sciences (the last row). (D) Design and synthesis of DNA tetrahedra and their AFM images. Reprinted with permission from ref. 32. Copyright (2005) American Association for the Advancement of Science. (E) Schematic and representative 2D nanoshapes formed by DNA origami. Reprinted with permission from ref. 36. Copyright (2006) Nature Publishing Group.

molecular scale positioning and patterning, thereby providing infinite possibilities for fundamental and bioapplication studies.

2.2 Dynamic DNA nanotechnology

The development of dynamic DNA nanotechnology is based on structural DNA nanotechnology. Whereas structural DNA nanotechnology obtains a final static structure, dynamic DNA nanotechnology aims at engineering smart nanomachines to fulfill sophisticated tasks based on dynamic DNA base-pairing.[15] The mechanism responsible for dynamic DNA nanotechnology consists basically of toehold-mediated strand displacement and the branch migration reaction (Fig. 2A). A ssDNA (in green) binds to a partially hybridized dsDNA via a short DNA domain that is typically 5–8 bases in length (termed the toehold), resulting in the release of the original complementary DNA by branch migration. The whole process is facilitated by the toehold and consists of a series of dynamic reversible single nucleotide dissociation and hybridization steps. The reaction rate and kinetic property can be regulated by varying the base number and components of the toehold domain, which is useful in the rational design of dynamic DNA nanomachines and improves our understanding of the kinetics of nucleic acid reactions.[41,42] This principle was initially used by Yurke to engineer a dynamic device, resulting in the

successful construction of reversible DNA tweezers.[43] Alternating incubation with fuel ssDNAs F and F̄ reversibly switched the configuration of the tweezers between the open and closed states (Fig. 2B). The coordinated motion of the device provided new opportunities in the design of more advanced nanomachines.

Inspired by Yurke's tweezers, more intricate DNA nanodevices, including DNA walkers,[44] DNA motors,[45] DNA machines[43] and DNA computing systems,[46] are under rapid development. They are anticipated to be widely used in both in vitro and in vivo settings. The DNA walker[47] is a notable example among the dynamic devices, and the walking dynamics have been carefully studied since its development.[48] With a deeper understanding of the kinetic properties of DNA molecules, a DNA robot system has been constructed to perform autonomous cargo sorting.[49] Additionally, it was reported that DNA nanorobots were able to interact with each other to execute specific functions in living animals.[50] Other real applications of these nanodevices include the regulation of enzymatic reactions using a DNA vault,[37,51] more reliable cancer cell line identification[52] and mRNA imaging in living cells.[53]

In addition to dynamic DNA nanodevices, cascade DNA reactions are also important research contents in dynamic DNA nanotechnology. In cascade DNA reactions, one trigger/initiator/target DNA molecule causes a series of cascade
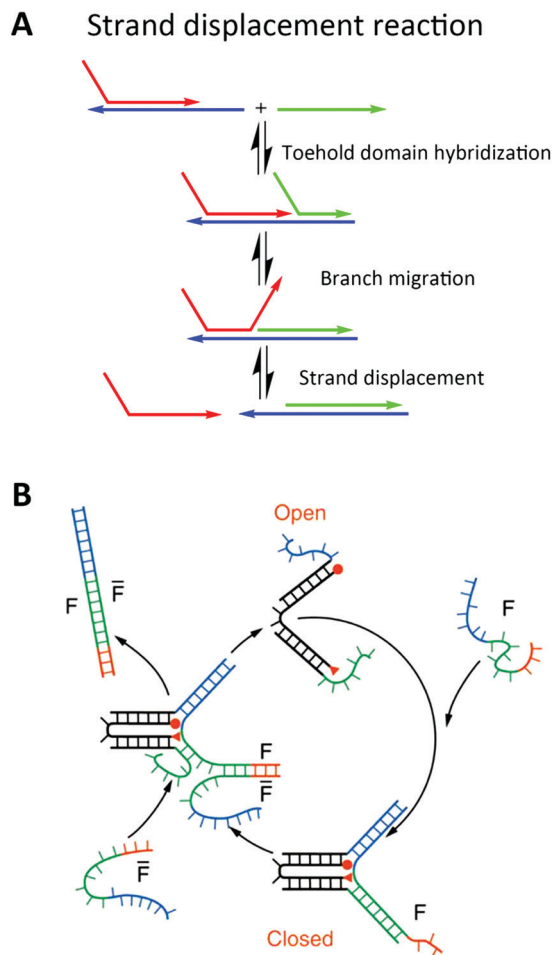
A Strand displacement reaction

B

Fig. 2 (A) Schematic of the toehold-mediated strand displacement and branch migration reaction mechanism. (B) Operation of reversible DNA tweezers. Reprinted with permission from ref. 43. Copyright (2000) Nature Publishing Group.

reactions rather than a single reaction as in dynamic DNA device systems. Three examples of basic elegant cascade reactions in dynamic DNA nanotechnology are the hybridization chain reaction (HCR), catalytic hairpin assembly (CHA) and the primer exchange reaction (PER). As shown in Fig. 3A, HCR is composed of two hairpin DNAs (H1 and H2) and a trigger DNA (I). The trigger DNA I sequentially and alternately opens the hairpin DNA by rational design, yielding a long nicked double-helical DNA nanostructure (I·H1·H2).[54] Owing to its intrinsic property of signal amplification, HCR has been widely used in sensitive biosensing and bioimaging.[55,56] The CHA reaction (Fig. 3B) also involves the hybridization of two hairpin DNAs (A and B) in the presence of a trigger DNA (I). In contrast to HCR, the trigger DNA can be spontaneously displaced and recycled during the assembly process, similar to a catalyst, resulting in numerous assemblies of two hairpins.[57,58] The final product of CHA is a short double helix of two hairpin DNAs, and the reaction efficiency is less restricted by the trigger concentration. Thus, CHA displays improved signal amplification performance with low background and high turnover rates. Due to the above

features, it has been widely used for various bioapplications, including the detection of nucleic acids and cell imaging.[59–61] The PER cascade (Fig. 3C) is a polymerase-aided ssDNA synthesis method. The reaction primer (a) hybridizes to the toehold domain (a*) of a PER hairpin probe. The extension of the primer at the 3′ end by polymerase (b) replaces the original complementary strand in the hairpin until inhibited by a stop sequence. The replaced domain competes with the copied domain through a random-walk process of three-way branch migration, leading to the dissociation of the extended primer, and finally appending the prescribed sequence of the hairpin to the primer strand. The extended primer is able to react with another hairpin probe to extend the sequence repeatedly.[62] Traditional ssDNA synthesis method produces identical copies of fixed sequences, whereas PER overcomes this limitation in a programmable and stepwise way, providing the basis for a new generation of DNA molecular circuits and devices.

The simple strand displacement reaction can trigger the dehybridization and rehybridization of the DNA double helix. When these DNA molecules are modified with functional groups, this particular dynamic process is a promising strategy to realize additional functions, including protein assembly,[63] microRNA imaging[64] and telomerase activity evaluation in living cancer cells.[65] Additionally, a series of higher-order structures have been constructed using a four-way toehold-mediated strand displacement reaction, demonstrating that hierarchical assembly can be achieved using dynamic DNA nanotechnology.[66] With these rapid advances in dynamic DNA nanotechnology, we anticipate that the interface can be engineered using the abovementioned reactions for the development of more bioapplications.

### 2.3 Functional DNA nanotechnology

In the field of functional DNA nanotechnology, the chemical functionality of DNA expands into new aspects beyond storing and transmitting genetic information. Aptamers and DNAzymes are two primary representative categories of functional DNAs, which are obtained from in vitro selection with specific binding affinity and catalytic capability, respectively.[14]

Aptamers, which are selected by the systematic evolution of ligands by exponential enrichment (SELEX) technology, can specifically bind to their targets with high affinity along with structural switching. The selection process has advanced from in vitro to in vivo and living animals.[67] Aptamers are widely used as sensitive biosensors,[68,69] bioimaging agents[70] and targeted therapeutics.[71] Recently, a tumor microenvironment targeting aptamer that simultaneously binds polymorphonuclear myeloid-derived suppressor cells and tumor cells has been successfully selected. The conjugation of the dual targeting capability aptamer to a chemotherapy drug displayed improved anticancer efficacy.[72] In comparison with monoaptamers, circular bivalent aptamers exhibit improved stability and molecular recognition ability, as illustrated by enhanced protein delivery efficiency into living cells (Fig. 4A).[73] Additionally, aptamer-based activatable photoacoustic imaging probes for thrombin have been successfully demonstrated in living cells (Fig. 4B), significantly expanding the application of aptamers.[74]

A Hybridization chain reaction (HCR)
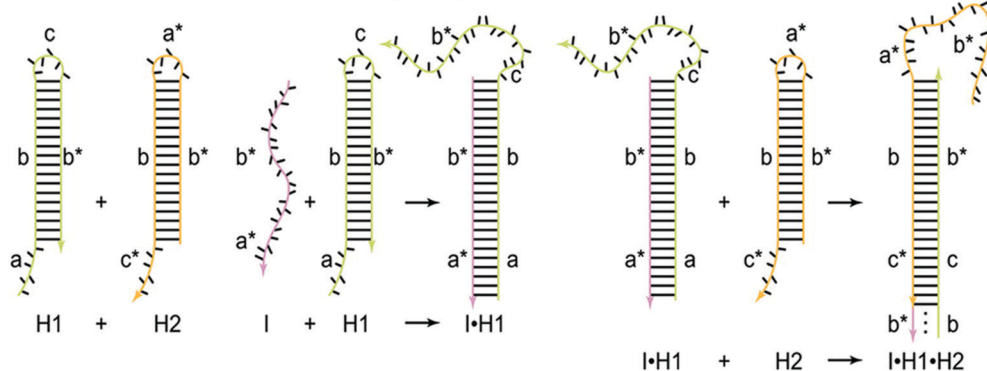
B Catalytic hairpin assembly (CHA)
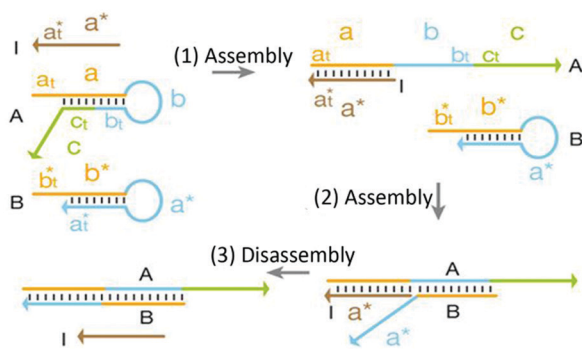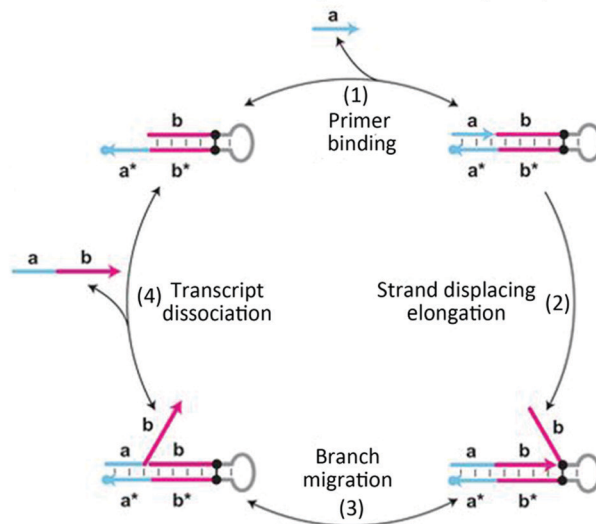

C Primer exchange reaction (PER)

Fig. 3 Schematic of the fundamentals of different DNA cascade reactions. (A) HCR. Reprinted with permission from ref. 54. Copyright (2004) National Academy of Sciences. (B) CHA. Reprinted with permission from ref. 58. Copyright (2008) Nature Publishing Group. (C) PER. Reprinted with permission from ref. 62. Copyright (2018) Nature Publishing Group.

DNAzymes are another set of functional DNA molecules with catalytic activity.[75,76] Among the developed DNAzymes, RNA-cleaving DNAzymes are particularly interesting because of their fast reaction rates and ease of practical application. They are obtained through a combinatorial process with specific metal ions as catalytic cofactors (Fig. 4C). The selection method is general to any specific metal ion species without requiring an advanced understanding of the properties of metal ions.[76–78] Typically, as depicted in Fig. 4C, the DNAzyme is composed of a substrate strand with an incorporated RNA cleavage site and an enzyme strand with a catalytic core domain. Upon binding the metal cofactor, the cleavability of the DNAzyme was used to construct *in vitro* heavy metal ion biosensors,[79] living cell metal ion imaging systems,[80,81] activatable DNA motors,[45,82] gene silencing[35] and theranostic systems.[83,84] The development of these functional DNA molecules has significantly broadened the research field of DNA nanotechnology, and the engineering of interfaces with these functional molecules has provided a range of interesting bioapplications.

Although we have split DNA nanotechnology into three branches, the most useful bioapplications are those that combine these branches. The combination of different DNA nanotechnologies has efficiently integrated their powerful functions, leading to numerous exciting prospects. For example, combining structural DNA nanotechnology (DNA origami) and functional DNA nanotechnology (DNA aptamer) enabled the engineering of a responsive *in vivo* therapeutic nanorobot,[85] and the combination of dynamic DNA nanotechnology (DNA walker) with functional DNA nanotechnology (DNAzymes) shows potential for drug delivery applications.[86]

3. Bioapplications of DNA nanotechnology at flat interfaces

Flat interfaces, including electrodes, glass slides, microfluidics, microchips and nanopores, are exploited as platforms in biosensing and biological diagnosis. Due to facile modification
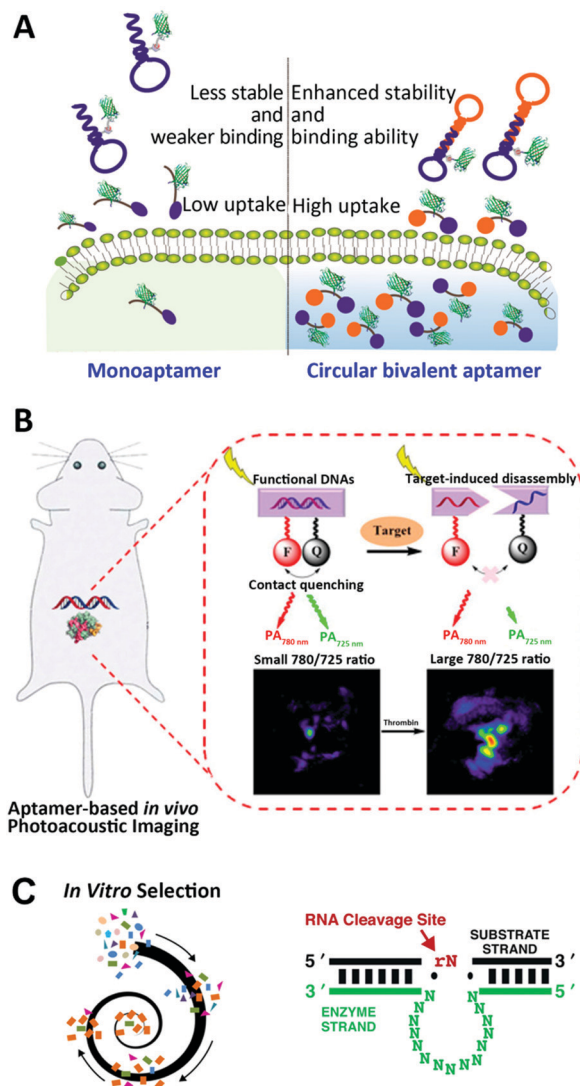
Fig. 4 (A) Equipping circular bivalent aptamers with supramolecular βCD for enhanced intracellular protein delivery compared with monoaptamers. Reprinted with permission from ref. 73. Copyright (2018) American Chemical Society. (B) DNA aptamer-based activatable photoacoustic probes for imaging in living mice. Reprinted with permission from ref. 74. Copyright (2017) American Chemical Society. (C) Schematic illustration of the selection process and structure of DNAzymes. Reprinted with permission from ref. 79. Copyright (2017) Elsevier.

and programmability features of DNA molecules, DNA nanotechnology provides a convenient strategy to control the properties of a biomolecule-confined interface. The target accessibility can be improved at the solid–liquid interface, thereby enabling a wealth of bioapplications, as summarized and discussed in this section.

3.1 Bioapplications of structural DNA nanotechnology at flat interfaces

3.1.1 Tailoring interface properties for improved biosensing using tetrahedral DNA nanostructures. Flat interfaces engineered with structural DNA nanotechnology have successfully produced tailored interfaces for improved biosensing. The study of electrode-based flat interfaces has been well documented

because electrochemical biosensing approaches exhibit distinct advantages, including simple operation, fast response, low cost, and excellent sensitivity. Analysis of numerous biomolecules has been realized, especially that of cancer related nucleic acids.[87]

The formation of an ideal DNA molecular recognition layer on the electrode interface is of utmost importance for the success of biosensing. Control of the biosensing interface properties is essential to obtain high reproducibility of the sensors. Although DNA molecules with a terminal thiol modification can be easily functionalized on a gold electrode *via* Au–S chemistry, the precise density of the DNA layer is technically difficult to control. Moreover, the nonspecific interaction between the gold surface and DNA base nitrogen atoms induces the strands to lie flat on the surface instead of standing upright as required, which limits the accessibility and hybridization efficiency of target sequences at the solid–liquid interface. Toward this end, Fan's group proposed the use of 3D DNA nanostructures as a "soft lithography" approach to engineer an electrode interface to precisely tune the thermo-dynamic behavior of DNA hybridization.[88] Specifically, they developed an electrochemical DNA biosensing surface by immobilizing rigid DNA tetrahedron probes on an electrode. Three vertices of the tetrahedron were modified with thiol groups to firmly anchor the structure to the Au surface, and the other vertex of the tetrahedron was appended with a pendent capture probe to hybridize with the target. The intrinsically highly ordered and upright orientation properties of the DNA tetrahedron made the biosensing surface more accessible to the target. Meanwhile, the platform exhibited high selectivity towards its complementary sequence in comparison with noncognate sequences.[89] As DNA can be easily programmed, the lateral spacing between pendent capture probes can be controlled precisely by modulating the size of the DNA tetrahedron (Fig. 5A). Increasing the side length of the DNA tetrahedron decreases the interprobe density, and the hybridization kinetics
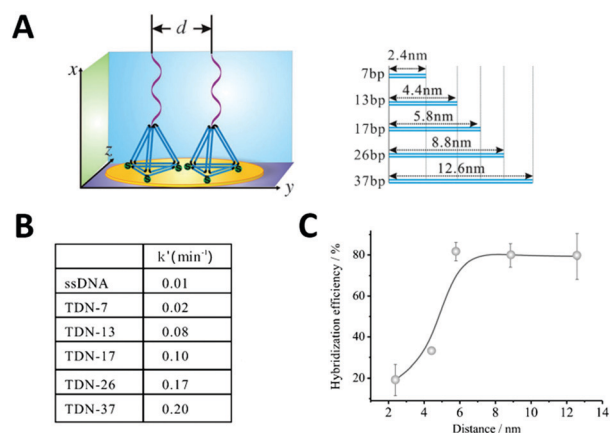

Fig. 5 (A) Precisely engineering the lateral distance between pendent probes by varying the size of the DNA tetrahedron. (B) The pseudo-first-order reaction rates corresponding to a series of DNA tetrahedra with varying sizes. (C) The hybridization efficiency corresponding to a series of DNA tetrahedra with varying sizes. All reprinted with permission from ref. 90. Copyright (2015) Wiley-VCH.

were improved 20-fold by varying the distance of the pendent capture probe from 1.8 to 12.6 nm (Fig. 5B). The hybridization efficiency was also increased five-fold by varying the distance from 1.8 to 6 nm (Fig. 5C).[90]

Simply changing the pendant probe sequence and this modification has customized the platform for the detection of a variety of targets, including tumor-necrosis-factor alpha,[91] cocaine,[92] microRNA,[93–96] prostate-specific antigen,[97] cancer cells,[98] H7N9 virus,[99] bacteria[100,101] and telomerase.[102] Due to the extensive influence of 3D DNA nanostructures, the Fan group comprehensively summarized the protocol using a DNA nanostructure-based biosensing interface to detect multiple targets in detail.[103] Theoretically, the engineered 3D DNA nanostructure biosensing interface is a versatile platform that can be adopted for other electrode surface-based detection methods. Researchers have also successfully employed DNA tetrahedra to construct electrochemiluminescence (ECL) biosensors to detect multiple targets, including telomerase[104] and oligonucleotides.[105,106]

Compared with traditional ssDNA-modified surfaces, the DNA tetrahedron engineered interface exhibits higher nonspecific protein resistance. Taking advantage of this property, Li et al. successfully demonstrated the direct detection of nucleic acids in complex media.[107] Instead of using the abovementioned tetrahedral DNA nanostructure with one pendent capture probe, they optimized the tetrahedral DNA with two pendent sensing strands from the vertices (Fig. 6). One pendent probe was the long recognition overhang that was distal from the electrode (Strand a) and the other pendent probe was the assisted short strand that was fixed near the electrode (Strand b). Upon binding with the target, the proximity of Strand a and Strand b caused an enhanced electrochemical signal because of the shorter distance between the electrochemical molecule and the electrode surface. This minor modification by using two pendent probes avoided multiple steps of incubation and washing during the detection process for the engineered DNA nanostructure interface, thereby greatly simplifying the operation and holding potential for in vivo diagnosis.

More interestingly, the incorporation of stimuli responsive molecules into DNA nanostructures can endow flat interfaces with a spatiotemporal activatable property. For example, Zhang and coworkers coupled a light-responsive 3D DNA nanostructure with an electrode to help solve the regeneration and reversible

locomotion challenge in biosensing and DNA nanotechnology.[108] In this work, azobenzene (azo)-functionalized DNA nippers were self-assembled into 3D DNA nanostructures and were further hybridized onto an electrode via a linker strand to form a well-engineered biosensing interface. The target microRNA was able to open the two nearby nippers to emit an enhanced ECL signal. Irradiation with UV light caused photoisomerization of the azo group to release the target. The engineered interface reverted to the initial state within 10 min. In another example, a pH-sensitive i-motif sequence was incorporated into the tetrahedral DNA to construct a proton-driven water pump on an elaborate interface. This DNA-based device could reversibly pump water and ferricyanide in a continuous-flow manner, as monitored by an electrochemical signal.[109]

We have summarized the biosensing applications using tetrahedral DNA nanostructure engineered electrode interfaces in Table 1. The detection of various targets, including small molecules, nucleic acids and proteins, has been achieved because of the easy programmability of DNA molecules. Their excellent detection performance is reflected by the impressive detection limits shown in Table 1. The 3D DNA nanostructure engineered electrode interfaces exhibit superior performance to that of traditional electrode interfaces for the following reasons: (i) the preparation of tetrahedral DNA nanostructures is simple and involves only one-step incubation. The high yield contributes significantly to the excellent reproducibility of the biosensing interface; (ii) these nanostructures are mechanically rigid and structurally stable. Such features enable the capture elements used to recognize targets to be arranged on the electrode interface in nanoscale precision. As a result, these biosensing interfaces are equipped with excellent target accessibility especially at the trace level; (iii) nonspecific protein adsorption is minimized, allowing direct detection in complex samples; and (iv) redox molecules can easily penetrate the hollow structure to access the sensing electrode to provide a sensitive detection signal.

These examples indicate that 3D nanostructures can be employed as useful tools to engineer biosensing interface properties for improved biosensing. The detection limit and the anti-interference capability in complex samples are both significantly improved, revealing high applicability in various biosensing applications. Additionally, by coupling structural DNA nanotechnology with flat interfaces, a series of stimuli sensitive devices with specific functions have been demonstrated, as reviewed above.

3.1.2 Tailoring interface properties for improved biosensing using DNA origami. DNA origami possesses intrinsic site-specific addressability with nanoscale precision. Taking advantage of this feature, two distinct DNA origami nanostructures starting from a 24-helix bundle building block were used to engineer a fiber optic surface plasmon resonance (FO-SPR) biosensing interface.[110] This was the first attempt to exploit DNA origami nanostructures to nanopattern an SPR biosensing interface. Specifically, as shown in Fig. 7A and B, DNA origami nanostructures were modified at either lateral surfaces (LS) or distal ends (DE) with two distinct groups of ssDNA: one group for anchoring at the biosensing interface and the other for specific hybridization of
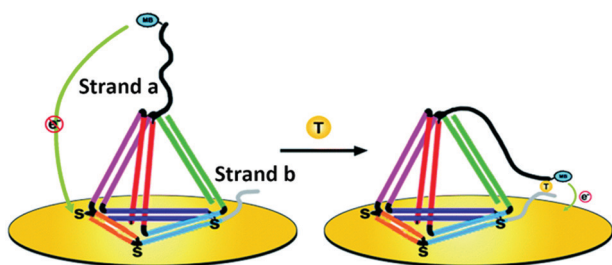

Fig. 6 Schematic of two pendent strand DNA tetrahedral-based electrode interface sensor. Reprinted with permission from ref. 107. Copyright (2018) Royal Society of Chemistry.

Table 1 Biosensing applications using tetrahedral DNA nanostructure engineered electrode interfaces

| Target/stimulus	Method	Signal transduction	Detection limit	Ref.
Tumor-necrosis factor alpha	Sandwich assay using HRP enzyme to catalytically reduce H_2O_2 in the presence of TMB	Electrochemical	100 pg mL^{-1}	91
Cocaine	DNA hybridization using HRP enzyme to catalytically reduce H_2O_2 in the presence of TMB		33 nM	92
microRNA-21	DNA hybridization using poly-HRP80 conjugate to catalytically reduce H_2O_2 in the presence of TMB		10 fM	93
microRNA-122b	HCR amplified assay using HRP enzyme to catalytically reduce H_2O_2 in the presence of TMB		10 aM	94
microRNA-141	Conformational change of hairpin DNA using HRP enzyme to catalytically reduce H_2O_2 in the presence of TMB		1 fM	95
let-7a	Rolling circle amplification-based assay using AgNPs as signal reporter		50 aM	96
Prostate-specific antigen	Sandwich assay using AuNP loaded numerous HRP enzyme molecules to amplify the signal		1 pg mL^{-1}	97
Cancer cells	Multibranched HCR amplified assay using HRP enzyme to catalytically reduce H_2O_2 in the presence of TMB		4 cells	98
H7N9 virus	DNA hybridization using HRP enzyme to catalytically reduce H_2O_2 in the presence of TMB		100 fM	99
Escherichia coli	Sandwich assay using ferrocene as signal reporter		1.20 CFU per mL	100
Streptococcus pneumoniae	Sandwich assay using ferrocene as signal reporter		0.093 CFU per mL	101
Telomerase	DNA hybridization with the telomerase elongation product using HRP enzyme to catalytically reduce H_2O_2 in the presence of TMB		10 cells	102
DNA	Target binding induced proximity using MB as signal reporter		300 fM	107
Telomerase	Dual-potential ECL assay using CdS QDs and luminol-modified AuNPs	ECL	1.49×10^{-9} IU	104
DNA	DNA cyclic amplified assay using Ru(bpy)$_3$$^{2+}$-conjugated silica nanoparticles as signal reporter		40 aM	105
DNA	CHA amplified assay using Ru(bpy)$_3$$^{2+}$ as signal reporter		20 aM	106
microRNA-21	Photoswitching reversible 3D DNA nanomachine assembled by azobenzene-functionalized DNA nippers using Ru(bpy)$_3$$^{2+}$ as signal reporter	ECL	6.6 fM	108
pH	I-motif incorporated DNA tetrahedral nanostructure using Fe(CN)$_6$$^{3-}$ as signal reporter	Electrochemical	—	109
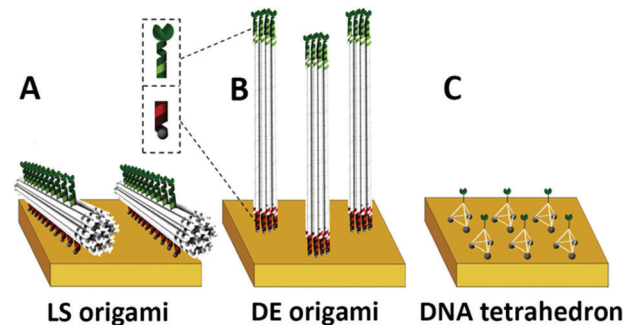
Fig. 7 Schematic of probe patterning at the flat gold interface using (A) DNA LS origami, (B) DNA DE origami and (C) DNA tetrahedron. Reprinted with permission from ref. 110. Copyright (2018) American Chemical Society.

capture probes. Thrombin capture probes were positioned with different densities by hybridization to the predefined staple strand overhangs. The distance of the capture probes from the biosensing interface was easily tuned by changing the orientation of the DNA origami nanostructure. When the DNA origami nanostructure was parallel to the surface, a distance of 27 nm was obtained (Fig. 7A), while a perpendicular orientation of the DNA origami nanostructure with respect to the surface exhibited a distance of 113 nm (Fig. 7B). The performance comparison of the DNA origami and tetrahedral DNA nanostructure patterned surfaces revealed that the widest linear range was obtained using the LS DNA origami nanostructure-oriented surface. Meanwhile, the LS DNA origami nanostructure yielded extremely high reproducibility, indicating the potential of DNA origami nanostructures for engineering interfaces for improved biosensing applications.

Zero-mode waveguides (ZMWs) consisting of small holes in a metal film are effective tools for excluding the influence of background molecules during single-molecule biosensing. Particularly, one target molecule should be positioned in one hole for better applications. To address this challenge, a DNA origami nanoadapter with appropriate size that can be accommodated in ZMWs was employed.[111] The single dye molecule was anchored at predefined positions on a disk-shaped DNA origami nanoadapter, and this DNA origami nanoadapter was placed successfully in one hole. This arrangement improved the photophysical properties of the dye molecules because the dye position was restricted to a defined area. Furthermore, similar ZMW-based technology was employed to study the interaction of dyes and metallic nanoparticles.[111]

The aforementioned designs exploit the structural property of DNA origami, seemingly underestimating the dynamic actuation capability of the 3D DNA origami. In this respect, Torelli et al. constructed a 3D DNA nanorobot engineered fiber optical biosensor. The closed 3D DNA origami hybridized with a gene target to open the flap and release the encapsulated molecules for signal readout, realizing the picomolar detection of the target within 90 min.[112] The successful demonstration of this proof-of-principle paves the way for different interfacial biosensing applications and point-of-care diagnosis using DNA origami nanostructures.

3.1.3 DNA nanostructure-assisted interface protein patterning.

Studying protein patterning is highly important for understanding the relationships among protein–protein and protein–cell interactions. Highly ordered self-assembled monolayers formed by DNA origami provide an effective approach for protein patterning. These surface-assisted monolayers can be obtained by either close-packing in the presence of monovalent cations or blunt-end stacking interactions between origami units.[113,114] Recently, the formation dynamics of DNA origami patterns at the solid–liquid interface have been studied thoroughly using high-speed atomic force microscopy imaging.[115] Based on these findings, highly packed hexagonal lattices with internal cavities were reported, by the assembly of triangular DNA origami tiles. They were used as molecular lithography masks on mica surfaces for protein patterning.[116,117] The protein coverage can be tuned from a single protein to multiple proteins by varying the buffer and adsorption conditions. The versatility of the proposed method was demonstrated using four proteins. Similarly, 2D arrays were constructed at the interfaces by blunt-end stacking for protein patterning.[118]

Despite progress, the instability of DNA origami nanostructures with respect to changes in pH, buffer conditions and temperature imposes drawbacks for this specific application, because the requirements for the stabilization of DNA origami nanostructures may not always be compatible with the stability of the protein to be patterned. To address this challenge, a so-called "single-molecule contact printing" strategy was proposed for the arrangement of streptavidin at the solid–liquid interface.[119] This approach employed a transfer process involving a site-addressable DNA origami carrier rather than directly using DNA origami nanopatterns. The gold surface is initially functionalized with 3,3′-dithiodipropionic acid (DTPA) to further conjugate with the amino group-modified DNA strands on the "DNA origami stamp" by a covalent reaction. Subsequent dehybridization of dsDNA strands "ink" ssDNA strands on the surface as anchors to further create single-molecule arrays with nanometer precision.

3.1.4 DNA origami hybrid nanopores for biosensing and biomedical applications.

Nanopores are powerful tools for single-molecule biosensing. Typically, nanopores are classified into two species: solid-state nanopores fabricated by either drilling a hole into a silicon-based flat membrane or laser-assisted pulling of a glass pipette into a glass nanocapillary and biological nanopores produced by inserting natural proteins into lipid bilayers. During the last decade, DNA origami hybrid nanopores have attracted extensive research attention due to their distinct advantages of tunable geometries and pore surface functionalities compared with traditional nanopores. The formation detail and properties of these hybrid nanopores have been summarized elsewhere.[120,121] In this section, we focus mainly on their demonstrated and potential bioapplications.

The most widely documented application of DNA origami hybrid nanopores is the detection of charged single molecules. In 2012, Bell *et al.* demonstrated for the first time the reversible insertion/ejection of a DNA origami nanostructure from a solid-state nanopore by electrophoretic translocation.[122] This result paved the way for combining DNA origami and nanopores.

In follow-up studies, either an integrated DNA origami nanoplate or a rectangular DNA origami nanoplate with different central aperture sizes was employed to cover the mouth of a solid-state nanopore for biosensing applications. Various designs of integrated DNA origami nanoplates were reported to display overall good permeability to ions. Under a driven force using high voltage, the nanoplates covering the nanopore can be pulled from one side to another.[123] By varying the size of the DNA origami central aperture, the DNA origami hybrid nanopore was able to discriminate protein molecules demonstrated by the drop of the ionic current signal. Simultaneously, the incorporation of specific ssDNA at the center of the DNA origami enabled single-molecule sensing of DNA snippets and genomic phage DNA.[123] The strategy has been demonstrated to be successful in DNA strand translocation by using glass nanocapillaries as well, which are easier to manufacture than silicon-based nanopores.[124]

It is known that membrane-spanning proteins insert into a lipid bilayer to control molecule and ion transport. Inspired by this construct, DNA origami nanostructures with appropriate hydrophobic modifications were utilized to insert into lipid bilayers to form channels. For example, a stem-barrel DNA origami nanopore was constructed to form a transmembrane channel in a lipid bilayer using a 26 cholesterol moiety tagged barrel cap.[125] The synthetic channels are used to sense the translocation of DNA strands, including single-stranded hairpins and G-quadruplexes.

The use of DNA origami hybrid nanopores in biomedical applications is another area of growing interest. Burns *et al.* developed several methods to incorporate different hydrophobic tags into self-assembled DNA bundle nanostructures with an inner channel.[126–128] These hydrophobic moieties, including tetraphenylporphyrin, ethyl phosphorothioate (EP) and cholesterol groups, enable the DNA nanostructure to span across the lipid bilayer. Among them, EP groups are toxic toward cancer cells, indicating potential applications in cancer therapy.[127] To further extend bioapplications, a controllable locking strand was integrated with the DNA bundle as a molecular gate to close the entrance of the channel. The improved nanostructure was further employed to form a membrane-spanning nanopore system. Upon binding to a ligand, the pore reopens to release the cargo for transport and controlled drug release.

3.2 Bioapplications of dynamic DNA nanotechnology at flat interfaces

3.2.1 Kinetic studies of DNA nanomachines.

DNA nanomachines were initially designed to perform sophisticated tasks in biological systems and to replace their naturally occurring counterparts; however, the stepping rates are relatively slow compared with native rates. For example, it took approximately 5 min for a DNA robot to finish a single cargo-sorting operation between a 6 nm neighboring foothold gap,[49] while the translocation rates for natural protein motors are 1 μm s^{-1} under saturating ATP concentrations.[129,130] Thus, more fundamental principles need to be uncovered to improve the performance of these nanomachines, and flat interfaces have played vital roles
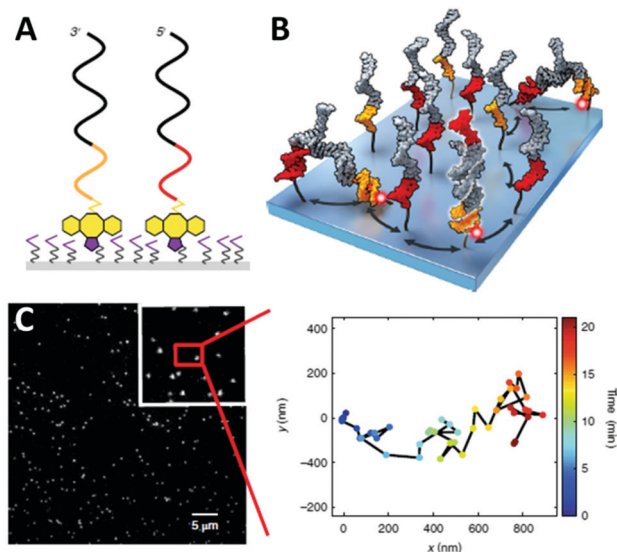
Fig. 8 (A) Schematic of two DNA footholds with alkyne terminals conjugated to a glass coverslip surface through copper-free click chemistry. Surface azides are displayed in purple and dibenzocyclooctyne (DBCO) in yellow. (B) Schematic of DNA walker movement at the functionalized interface over a 2D array of footholds. (C) TIRF image of a fluorophore labeled walker on a premodified surface and a representative fast-moving trajectory of the walker. All reprinted with permission from ref. 131. Copyright (2018) Nature Publishing Group.

Fig. 9 (A) Schematic of the microfluidics experimental setup. DNA walker tracks are immobilized inside the chamber through biotin–neutravidin interactions. (B) Schematic of the walking process of a DNA bipedal walker and the operational yield comparison between two operation models. All reprinted with permission from ref. 132. Copyright (2017) American Chemical Society.

for this specific requirement. For example, a glass coverslip was employed as a substrate to engineer the interfacial toehold exchange reaction to explore the speed limit of a DNA nanomachine.[131] Two kinds of alkyne-modified footholds were attached to the azide-modified glass coverslip *via* click chemistry (Fig. 8A), generating a random, high-density functionalized interface and allowing the movement of a DNA walker (Fig. 8B). By optimizing the length of the toehold domain and branch migration domain, the stepping rate was improved by more than an order of magnitude, which was characterized by single-molecule fluorescence resonance energy transfer (sm-FRET). The fastest walker, with a 6-nt toehold length, exhibited translocation speeds of ~ 300 nm min^{-1}. In contrast, a walker with a toehold length of 8 nt had a translocation speed of ~ 13 nm min^{-1}. In combination with fluorescent molecules, the walking trajectory can be readily tracked on flat interfaces by total internal reflection fluorescence (TIRF) microscopy (Fig. 8C). With the help of the confined flat interfaces, the rational optimization was demonstrated to improve the performance of the DNA nanomachine, which is not limited by fundamental strand displacement reactions.

The flat interface also helps to address another limitation of fuel-triggered DNA nanomachines, namely, the gradually reduced processivity caused by the interference of accumulated fuel strands. In this regard, a microfluidic interface was employed for automatic introduction and removal of fuel strands controlled by computer.[132] Specifically, the DNA walker track was immobilized onto the coverslip *via* a biotin–neutravidin interaction (Fig. 9A). The sequential addition of nine fuel strands and eight corresponding anti-fuel strands caused the DNA walker
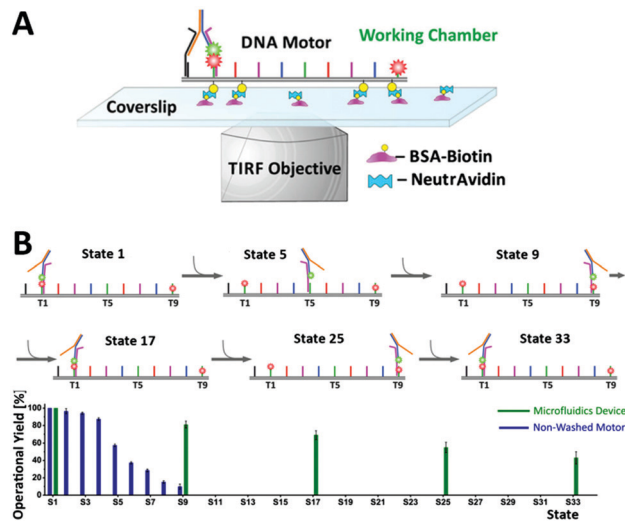
to operate from State 1 to State 9, as monitored by single-molecule FRET. Only eight walking steps could be reached in a homogeneous solution because of the toxic effect caused by the accumulation of the fuel and anti-fuel strands. On the other hand, with the help of microfluidic interfaces, the operational yield and processivity increased six-fold (Fig. 9B).

Owing to the advanced microscopy technology, rationally engineered flat interfaces by dynamic DNA nanotechnology enable the high time resolution capture of cascade reaction kinetics and single-molecule machine monitoring. The obtained knowledge will guide the design and construction of DNA nanomachines and DNA motors with improved operation processivity.

3.2.2 Signal amplification for biosensing. Given the intrinsic signal amplification capability of dynamic cascade DNA reactions and DNA walkers, as illustrated in Section 2.2, they are frequently utilized to engineer flat interfaces for amplified biosensing.

Dynamic cascade DNA reaction, like HCR, enabled the formation of long DNA double helix structures triggered by the target, which is regarded as a useful strategy to amplify biosensing signals. The conjugation of different readouts, including electrochemical small molecules (*e.g.*, hexaammineruthenium(III) chloride, methylene blue) and metal ions, allowed the sensitive detection of a variety of targets. Hexaammineruthenium(III) chloride ($[Ru(NH_3)_6]^{3+}$, RuHex) is a positively charged electrochemical indicator that intercalates into the negatively charged DNA double helix. Taking advantage of this property, Chen *et al.* constructed a DNA self-assembly amplified interface and RuHex was used to indicate the electrochemical signal to sensitively detect viral DNA at concentration as low as 5 aM.[133] Because of the easy programmability of DNA, this amplification strategy can be readily combined with other amplification methods, such as target recycling[134] or nanoparticle-based
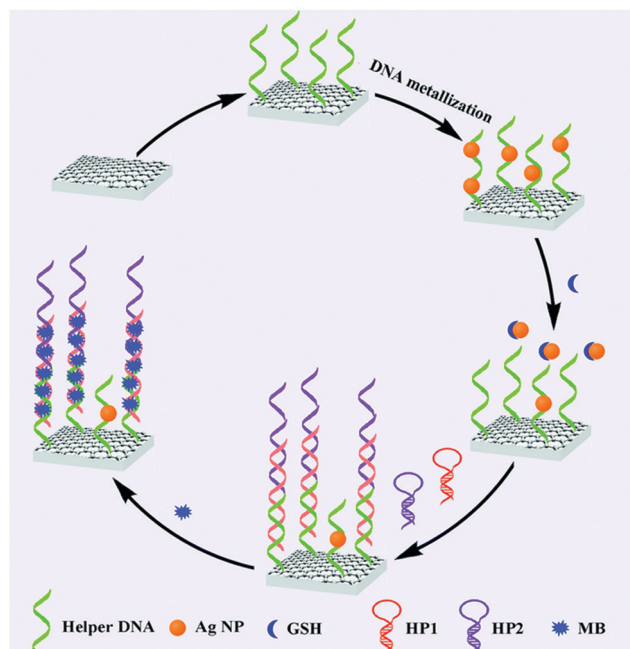
Fig. 10 Schematic of a ratiometric electrochemical biosensor using MB and metal nanoparticles as signal reporters for GSH detection. Reprinted with permission from ref. 138. Copyright (2017) Royal Society of Chemistry.
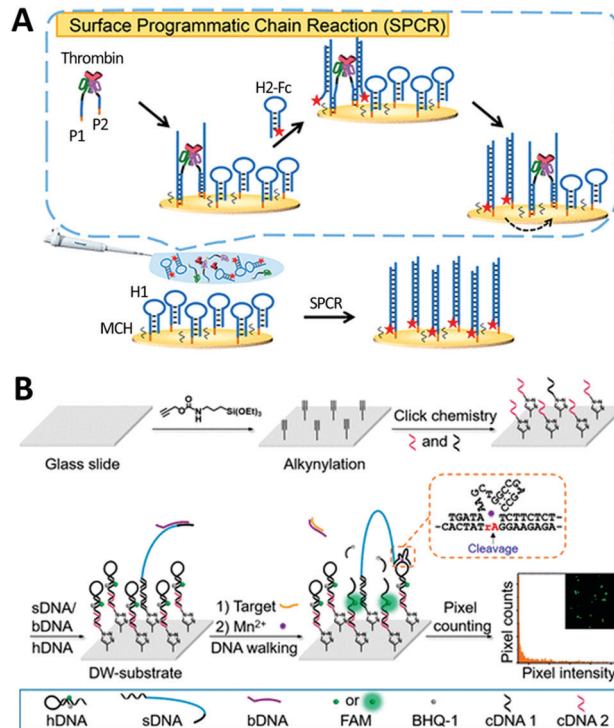

Fig. 11 Schematic of (A) a bipedal DNA walker–powered electrochemical biosensor for the amplified detection of thrombin. Reprinted with permission from ref. 143. Copyright (2018) American Chemical Society. (B) DNA walker-based pixel counting strategy for the amplified detection of nucleic acids. Reprinted with permission from ref. 144. Copyright (2018) American Chemical Society.

amplification,[135,136] to detect nucleic acids at concentration as low as 0.36 fM, telomerase activity in two HeLa cells and microRNA at concentration as low as 2 aM. Due to their strong binding ability to DNA, metal nanoparticles are also widely used as an electrochemical signal readout for DNA assemblies. Compared with electrochemical intercalating small molecules, a single metal nanoparticle containing countless metal ions is considered to be a signal amplifier itself. Yang et al. proposed a strategy that used target-triggered HCR assemblies at a flat interface for microRNA analysis. The electrochemical signal was generated by silver nanoclusters which was reduced beforehand on hairpin sequences. The detection limit for miRNA-199a in this assay was 0.64 fM.[137] In a recent report, methylene blue (MB) and metal nanoparticles were simultaneously used to construct a ratiometric biosensor (Fig. 10). In this study, DNA that was bound with silver nanoparticles was unable to hybridize with its complementary counterparts. In the presence of target glutathione (GSH), silver nanoparticles were released and the blocked DNA initiated HCR on the electrode to yield an increased MB signal and a decreased silver signal. The current ratio (I_{MB}/I_{Ag}) was employed to monitor intracellular redox homeostasis via the GSH level.[138]

In contrast with the abovementioned linear DNA self-assemblies, nonlinear DNA self-assemblies are expected to exhibit superior amplification performance; therefore, they have drawn considerable attention in flat interface amplified biosensing recently. For instance, Chang and coworkers reported a DNA hydrogel-based turn-off sensor for PDGF detection. In that work, a multibranched HCR reaction triggered by PDGF would form a DNA hydrogel which contained opened hairpin DNA. The hydrogel can be subsequently captured on the

electrode via exposed hairpin DNA, leading to the inhibition of the electrochemical signal generated from conducting material modified at the electrode surface. The high efficiency of the DNA hydrogel as an electron blocker made it possible to achieve a detection limit as low as 3.5 fM.[139] Moreover, DNA dendrimers formed by a tetrahedron self-assembly were reported as a carrier to load a large amount of the ECL indicator to amplify the detection signal.[140] Additionally, amplified nucleic acid sensing using quartz crystal microbalance (QCM) and amplified fluorescence sensing of cells were achieved based on DNA-streptavidin dendrimers on the flat interface.[141,142]

Typically, signal amplification engineered at the flat interface based on the above dynamic cascade reactions is a two-step reaction including the capture of the trigger strand and the cascade reaction for signal amplification, which is time consuming. In contrast, the DNA walker-based approach is a one-step incubation method; as a result, it has been widely used for engineering intelligent interfaces for amplified biosensing. For example, Zhu and coworkers proposed a bipedal walker powered electrochemical biosensor for the sensitive detection of a protein (Fig. 11A). Taking thrombin as a model, they split the specific aptamer into two parts called P1 and P2. One-step incubation of thrombin with two partial aptamers formed the bipedal DNA walker. One split aptamer cannot hybridize with the hairpin DNA 1 (H1) tethered on the electrode, whereas the bipedal DNA walker can bind to the electrode because of the

proximity effect. The introduction of the ferrocene-labeled hairpin DNA 2 (H2) replaced the walker leg through a toehold mediated strand displacement reaction. Therefore, the walker traversed the sensing interface to form abundant duplex structures of H1–H2 and eventually generated an amplified ferrocene electrochemical signal.[143] Instead of measuring electro-chemical signals, the pixel counting of fluorescent spot detection strategy was reported by Zhu et al. (Fig. 11B). In this study, two kinds of ssDNA strands were modified on the glass slide through click chemistry. Subsequently, a hairpin DNA (hDNA) comprising an RNA-cleaving DNAzyme substrate sequence was hybridized with one type of ssDNA as the track. A swing strand (sDNA), composed of a blocked enzyme sequence, was hybridized with another type of ssDNA as the walker. The target nucleic acid replaced the blocker which initially hybridized with sDNA via strand displacement reaction and the activated enzyme strand recombined with the substrate strand. In the presence of Mn^{2+}, continuous cleaving and binding operations were initiated, powering the walker to amplify the quenched fluorescence signal. The recovered fluorescent spots were digitalized as pixels using software and the number was found to show a positive correlation with the target concentration.[144] Notably, the detection processes based on DNA walker signal amplification involve only one-step incubation.

Table 2 summarizes the signal amplification strategies using dynamic DNA nanotechnology at the flat interface in more detail. The principles can be divided into two categories: dynamic DNA cascade reactions (including linear DNA assemblies with limited signal amplification capability and nonlinear DNA nanostructures with improved amplification performance) and DNA walkers. The signal transduction can be electrochemical, ECL, QCM or fluorescent. Interfacial dynamic DNA nano-technology enabled amplification strategies exhibit the advantages of easy-to-operate procedures, low false positive signals and high sensitivity. The application of dynamic DNA nanotechnology at flat biosensing interfaces has significantly increased our bioanalysis choices.

3.3 Bioapplications of functional DNA nanotechnology at flat interfaces

The immobilization of functional DNA molecules on flat interfaces is regarded as the first step toward the development

of commercialized portable biosensing devices. In addition to providing an immobilization platform, the flat interface also confers regeneration and long-term storage capabilities on the biosensors. The immobilization of Pb(ii)-specific DNAzyme on the gold surface was found to lower the detection limit from 10 to 1 nM without sacrificing the activity and specificity compared with solution-based systems.[145] A systematic study of the surface immobilization parameters, including the pore size of the gold-coated nanocapillary array membranes, the backfilling strategy and the reaction conditions of DNAzymes, has formed a firm basis for the real application of DNAzymes to monitor Pb^{2+} in municipal water systems.[146,147] Notably, no real effort has been spent on studying the use of 3D DNA nanostructures to tailor the properties of DNAzyme-based flat surfaces. We anticipate that the combination of DNA nanostructures with DNAzymes could further improve the biosensing performance of flat interfaces. Because DNAzymes consist of two strands (substrate strand and enzyme strand), with one strand modified at the interface, the other is free to conjugate with nanoparticles, thus facilitating novel biosensing principles[148] and assembly of 2D colloidals.[149] Similarly, structure switching aptamers have been immobilized at the electrode surface to detect a variety of targets, even in whole blood and the living body,[150–153] demonstrating their great potential to be commercialized for wider applications.

4. Bioapplications of DNA nanotechnology at nanoparticle interfaces

The precise geometric assembly of nanoparticles and modification of surface properties have been reported by incorporating DNA nanotechnology into nanoparticle research. Nanoparticles with large surface areas, good biocompatibility, high stability, and excellent physical and chemical properties are ideal candidates as carriers to engineer smart DNA walker/motor, activatable aptamers and DNAzyme-based systems that respond to stimuli for biosensing, bioimaging and biomedical applications both in vitro and in vivo. In this section, we will review these developments in DNA nanotechnology engineered at the interfaces of

Table 2 Signal amplification strategies using dynamic DNA nanotechnology at flat interfaces

Principle	Strategy	Signal transduction	Signal molecule	Target	Detection limit	Ref.
Dynamic cascade DNA reaction	Linear HCR	Electrochemical	RuHex	Virus DNA	5 aM	114
	Linear HCR	Electrochemical	Metal ions	microRNA-199a	0.64 fM	118
	Linear HCR	Electrochemical	MB and metal ions	GSH	103 pM	119
	Multibranched HCR	Electrochemical	Ferrocene	PDGF	3.5 fM	120
	Tetrahedron dendrimers	ECL	Doxorubicin conjugated N-(aminobutyl)-N-(ethylisoluminol)	Lipopolysaccharides	0.18 fg mL^{-1}	121
	DNA-streptavidin dendrimers	QCM	—	P53 gene	23 pM	122
	DNA-streptavidin dendrimers	Fluorescent	SYBR Green I	HeLa cells	4.4×10^3 cells per mL	123
DNA walker	Bipedal walker	Electrochemical	Ferrocene	Thrombin	0.76 pM	124
	DNAzyme-powered walker	Fluorescent	FAM	Nucleic acid	81 fM	125

nanoparticles and show their immense contributions to the diversity of bioapplications.

4.1 Bioapplications of structural DNA nanotechnology at nanoparticle interfaces

As scaffolds, 3D DNA nanostructures have been reported to guide the precise geometric assembly of nanoparticles with special physical properties. Applications have been substantially explored recently, especially for *in vivo* studies. For example, four kinds of nanoparticles were placed at four corresponding vertexes of a DNA tetrahedron, forming a chiral nanopyramid.[154] The nanopyramid recognized an intracellular miRNA and began to disassemble the nanostructure in real time.[155] Based on the change of the plasmonic circular dichroism (CD) signal, the strategy was even more sensitive than fluorescence-based detection to evaluate miRNA, indicating its potential for the detection of low-abundance biomarkers in cells.

Noble-metal based plasmonic nanoparticles possess environment-dependent optical properties, reflected by a shift of the localized surface plasmon resonance (LSPR) scattering spectrum peak. Engineering the interface of an Au@Ag core–shell nanocube with a tetrahedral DNA nanostructure facilitated the formation of such a plasmonic probe. The probe was employed to detect miRNA at the single-molecule level simply based on strand hybridization, and a LSPR scattering spectral wavelength shift of 0.4 nm was observed. Impressively, this platform allowed aM-level sensitivity for miRNA detection.[156]

The attachment of 3D DNA nanostructures to nanoparticles has addressed a significant challenge for particle functionalization. First, site-specific engineering of chemical functionality of nanoparticles is difficult to realize and structural DNA nanotechnology provides a simple, convenient and efficient way to achieve this goal. Different 3D nanostructures were initially attached to gold nanoparticles (AuNPs) as templates. After partial removal of the 3D DNA nanostructures, specific DNA strands remained at predefined locations of the AuNPs, endowing the AuNPs with site-specific assembly capability.[157] Second, phase transfer is typically required for further bioapplications of hydrophobic nanoparticles, but is difficult to achieve. For example, iron oxide nanoparticles (IONPs) have attracted extensive interest for magnetic resonance imaging (MRI) and sensor bioapplications due to their superparamagnetic properties.[158] To obtain highly uniform IONPs during the synthesis process, nonpolar solvents with high boiling point are usually involved, leading to coating of the hydrophobic ligands on the final product, which is not compatible with further bioapplications. As a solution, a structural DNA nanotechnology-based phase-transfer method has been proposed. In this study, a Janus DNA tetrahedral nanostructure was employed.[159] The tetrahedral nanostructure was composed of three carboxyl group terminated vertices and one aptamer overhang vertex. Because carboxyl groups bind Fe^{3+} with strong affinity, phase transfer of prepared IONPs can be realized easily from the oil phase to the water phase by the binding between tetrahedral DNA and IONPs. Interestingly, the biofunctionalities provided by aptamer were simultaneously conferred on the hydrophobic nanoparticles.

4.2 Bioapplications of dynamic DNA nanotechnology at nanoparticle interfaces

The bioapplications of dynamic DNA nanotechnology at nanoparticle interfaces are similar to those at flat interfaces. However, because of the wide choice of nanoparticle species with different chemical compositions and physical properties, the scope of bioapplications is much broader. For example, by coupling the superparamagnetic properties provided by magnetic nanoparticles (MNPs) and excellent signal amplification capability provided by dynamic DNA nanotechnology, a series of sensitive biosensing platforms with high separation capability have been reported.[160,161] By coupling nanoparticles with excellent fluorescence quenching ability, a simple strand displacement mechanism was used to image biomolecules in living cells based on the recovery of fluorescence.[162–164] We will summarize the bioapplications of dynamic DNA nanotechnology at nanoparticle interfaces in the following three sections.

4.2.1 Kinetic study of DNA walkers. DNA walkers engineered at the interface of fluorescent nanomaterials enable the direct visualization of the translocation of a single walker, which can provide kinetic information. For example, a near-infrared fluorescent carbon nanotube was used to noncovalently absorb DNAzymes (Fig. 12A). CdS fluorescent nanocrystals were used as walking labels to monitor the dynamic process.

With the addition of Mg^{2+}, the cleavage of the 10–23 DNAzyme substrate initiated the walking of CdS labels. The translocation trajectory was observed by fluorescence to be unidirectional with an average velocity of 1 nm min^{-1} (Fig. 12B).[45] In their follow-up study, single-walker behaviors were investigated with the aid of the super-resolution NIR technique using similar principles.[165] The fluorescent nanoparticles functioned as traditional nanocarriers and as fluorescent labels to monitor the DNA walker kinetics, facilitating intracellular biosensing and our understanding of DNA walker mechanisms.

4.2.2 On-particle DNA nanodevices for biosensing. On-particle DNA nanodevices formed from immobilizing rationally designed DNA sequences at the interfaces of nanoparticles have drawn significant attention because of their potential to execute specific functions, especially in living cells.
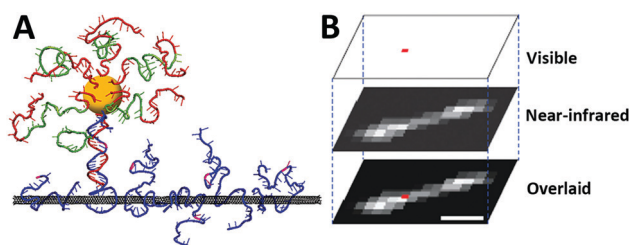

Fig. 12 (A) Schematic of a CdS nanoparticle-functionalized, 10–23 DNA-zyme based motor on the NIR fluorescent carbon nanotube track. (B) Fluorescence image. The pseudo-colored fluorescence image of the CdS nanocrystal (top) is overlaid with the near-infrared nanotube image (middle). The location of the mobile nanoparticle relative to the immobile nanotube (bottom) is periodically determined as a function of time during the experiments. Scale bar, 2 mm. All reprinted with permission from ref. 45. Copyright (2013) Nature Publishing Group.

AuNPs with interesting size and shape dependent plasmonic properties are widely used as highly efficient quenchers of multiple fluorophores and as localized heat generators upon appropriate light irradiation.[166] AuNPs are easy to modify by DNA using Au–S and Au–N chemistry and electrostatic interactions, thereby providing an ideal platform for the engineering of DNA nanotechnology at the interface. These particles are also biocompatible and easily internalized into mammalian cells. Based on these excellent properties, AuNPs have been of special interest for the study of interfacial DNA nanotechnology. The simple immobilization of ssDNA onto AuNPs not only improves the cell uptake efficiency but also increases the stability of ssDNA in complex media and accelerates the reaction kinetics of DNA hybridization.[7] This finding provided the foundation for more intensive studies and the exploration of more elegant bioapplications.

The high loading capability of AuNPs has allowed improvement of the mobility and efficiency of on-particle DNA nanodevices.[167] In an early example, an *in vitro* on-particle DNA motor biosensing platform was proposed.[168] As shown in Fig. 13A, the target recognition probe (L1) and the fluorescent indicator (S1) were anchored on AuNPs. In conjugation with target molecules, the

strand displacement reaction was triggered when the swing arm in a homogenous solution approached the AuNP probe. Subsequently, the addition of a nicking endonuclease caused iterative cleavage of S1 around the whole AuNP, leading to an increase in fluorescence which reflects the target molecule level. The length of DNA corona should be carefully optimized to obtain the best biosensing performance. This is the first demonstration of a 3D AuNP-based DNA walker; however, the nanodevice is limited to molecules with two binding sites or the sandwich binding model. Moreover, the design is not compatible with intracellular studies because the components need to be delivered separately into cells, which is complicated and restricts the reaction efficiency by decreasing the encounter possibility of the interacting components in the complex cellular environment.

In a follow-up study, these issues were solved by engineering all components on the surface of a single AuNP.[82] The blocked enzyme strands (S2) and RNA incorporated substrate strand (S1) were modified on the AuNP *via* Au–S chemistry (Fig. 13B). Incubation of the probes with cells caused the internalization of the probe. Overexpressed miRNA in cancerous cells competed with the locking strand *via* toehold-mediated hybridization,
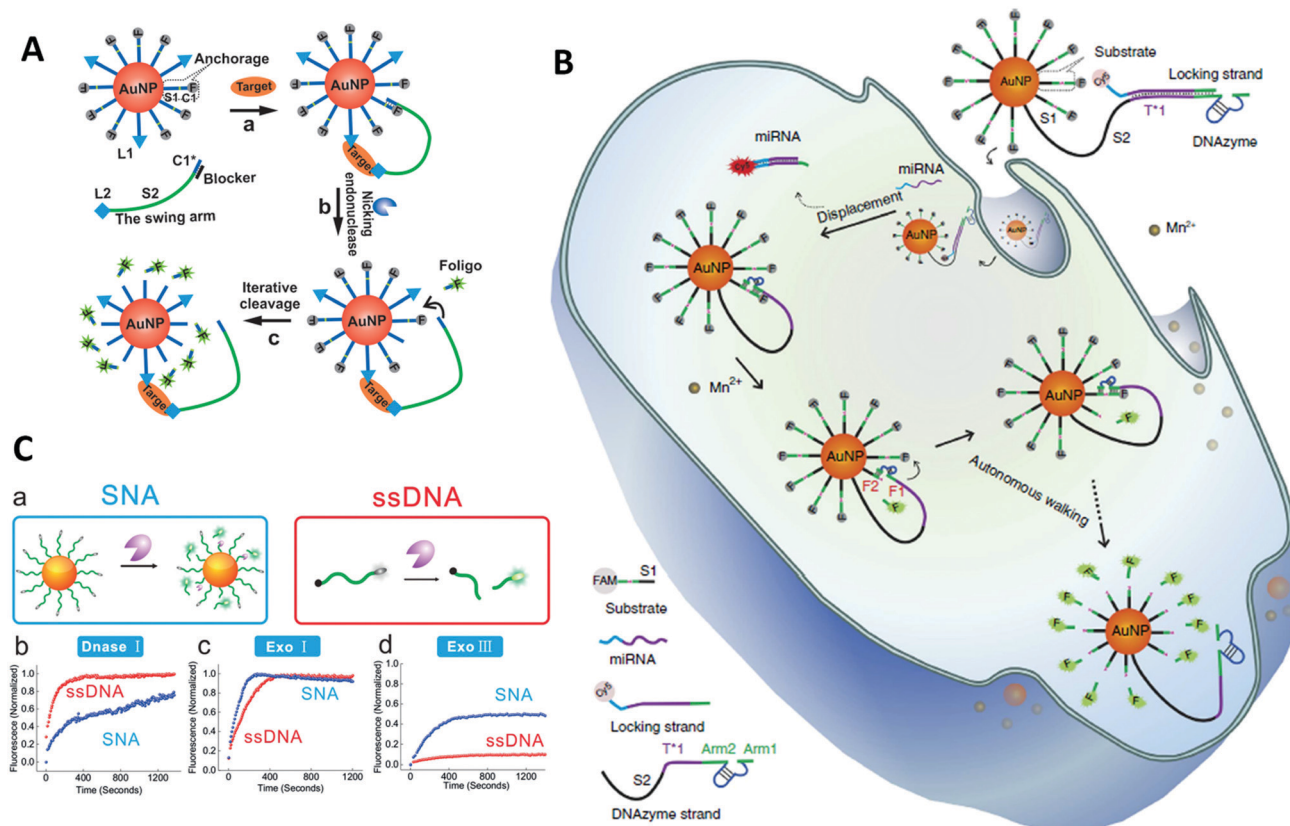

Fig. 13 (A) Binding-induced, on-particle DNA motor based biosensing platform. Reprinted with permission from ref. 168. Copyright (2015) Wiley-VCH. (B) Intracellular operation of an on-particle DNAzyme motor initiated by miRNA. Reprinted with permission from ref. 82. Copyright (2017) Nature Publishing Group. (C) Comparison of nuclease activities (DNase I, Exo I, and Exo III) toward SNA and free ssDNA. (a) Schematics of the fluorescence assays for hydrolysis of SNA and ssDNA. AuNP, nuclease, quencher, and fluorophore are depicted as yellow balls, purple dots, black dots, and green stars. (b–d) Fluorescence analysis of DNA hydrolysis by (b) DNase I, (c) Exo I, and (d) Exo III (ssDNA, red; SNA, blue). Reprinted with permission from ref. 171. Copyright (2017) Wiley-VCH.

releasing the caged enzyme strand to form active DNAzymes by hybridizing with the substrate. In the presence of metal ions, the active DNAzyme constructs triggered cleavage around the AuNP to release fluorescent molecules. Compared with the previously engineered model, this improved AuNP DNA nanodevice carrying all the components together favored cellular uptake and the intramolecular reaction. The operation speed was also enhanced by a local increase in the concentration of the components. More recently, nicking endonuclease enzyme powered on-particle DNA walkers have expanded the application scope to release payloads and detect nucleic acids.[169]

To achieve the desired performance, the engineering of DNA coronas for automatic operation is often based on iterative empirical sequence optimization, which requires additional labor and cost. To further engineer the on-particle DNA walker to discriminate single-nucleotide variants (SNA), a computer-guided simulation was proposed.[170] As an important parameter, the standard free energy ΔG for the strand displacement reaction was employed to balance the trade-off between the DNA nanomachine operation efficiency and specificity. A higher ΔG indicated excellent DNA nanomachine operation efficiency and poor specificity for discriminating SNA and vice versa. With the help of this simulation method, the discrimination factor for the target sequence and single nucleotide mismatch sequence improved by 5.4 times. This finding provides a strategy to rationally engineer 3D on-particle DNA nanodevices with optimal operation for wider bioapplications.

The abovementioned on-particle DNA walkers are based exclusively on the burnt-bridge mechanism using either endonuclease or DNAzyme hydrolysis of the walker track. Compared with the hydrolysis rate of endonucleases and DNAzymes, that of exonuclease III (Exo III) is 100–1000 fold higher. Taking advantage of this property, an Exo III powered DNA walker was successfully engineered.[171] The 3′ track was catalyzed to stepwise remove mononucleotides upon hybridization with the walker. Surprisingly, Exo III exhibited completely different hydrolysis behavior from that of DNase I and exonuclease I (Exo I). Exo III also showed higher hydrolysis activity toward SNA (Fig. 13C), illustrating its superiority in constructing a fast on-particle walker.

In addition to enzymes, an entropy powered on-particle DNA walker was also rationally engineered without requiring hydrolysis.[172] A series of DNA sequences were designed to initiate sequentially toehold mediated strand displacement reactions upon the recognition of target miRNA, thereby realizing intracellular imaging. Besides, endogenous ATP molecules were recently employed as a stimulus to power on-particle DNA nanomachines to image miRNA in living cells.[173]

4.2.3 Pore opening for drug release based on strand displacement reaction. Porous nanoparticles such as mesoporous SiO_2 nanoparticles (MSNs) and metal–organic-frameworks (MOFs) are considered ideal molecule-hosting candidates because of their tunable pore sizes, large surface areas, high loading capacity and well-defined surface properties.[174] Recently, stimuli-activatable, porous nanomaterial-based payload releasing platforms have drawn extensive research attention in biosensing[175]

and drug delivery.[176,177] Strand displacement reactions were used as a versatile strategy for pore opening, upon responding to specific biomolecular stimuli for controllable release.

For example, an "on-demand" drug release system was constructed and activated by an intracellular cancer biomarker.[178] In more detail, a partially hybridized dsDNA composed of a flexible long ssDNA and a short ssDNA was absorbed onto positively charged MSNs via electrostatic interactions to tightly seal the drug carrier. The overexpressed tumor marker (surviving mRNA) in cells hybridized with the long ssDNA via the toehold-mediated strand displacement reaction, leading to the formation of a rigid duplex that was unable to cap the pore. Therefore, the encapsulated drug molecules were released and the release efficiency was monitored by fluorescence recovery. In another example, the cascade DNA strand displacement reaction was engineered to take place at the interface of MSNs in a designated manner to open a pore.[179] Two-nanometer duplex DNAs formed by four ssDNAs were grafted directly onto the interface of MSNs via amide condensation to cage the 2.5 nm pores. Only the correct addition order of ssDNA initiated the cascade strand displacement reaction to leave subnanometer ssDNA on the interface. Finally, the subnanometer ssDNA was too small to cage the pore, and the signal indicators were released to indicate correct logical operations.

4.3 Bioapplications of functional DNA nanotechnology at nanoparticle interfaces

4.3.1 Intracellular imaging. With the development of functional DNA nanotechnology, RNA-cleaving DNAzymes and structure-switching aptamers were also used to engineer the surface of AuNPs. Delivering these molecules into mammalian cells to execute multiple functions became possible. For example, a DNAzyme–AuNP probe was developed to image the intracellular uranyl ion (Fig. 14A).[180] The probe was constructed by immobilizing a fluorophore modified DNAzyme onto AuNPs with the fluorescence readily quenched by the AuNP. Once the probe entered into cells and encountered uranyl, the substrate strands were cleaved and released the short fluorophore modified strand, leading to an increase in the fluorescence signal. This was the first demonstration of DNAzymes in an intracellular application. However, a drawback is that the DNAzyme biosensors can react with extracellular metal ions and cleave their substrate during the sensor delivery process before the sensors can reach the desired location in cells. A photocage method was then proposed to overcome this issue.[80] Initially, 2′-OH of adenosine ribonucleotides was conjugated with a UV light sensitive photocage group to inhibit the activity of DNAzymes. Only under the irradiation of UV light can the photocage group be removed, and the catalytic activity of the DNAzyme recovered. The photocaging method has been demonstrated in different systems[81] but requires high energy UV irradiation that can potentially harm cells.

More recently, an alternative near-infrared (NIR) photothermally activated method has been proposed using gold nanoshells (AuNS).[181] As shown in Fig. 14B, the system consists of a three-stranded DNAzyme precursor (TSDP) whose hybridization
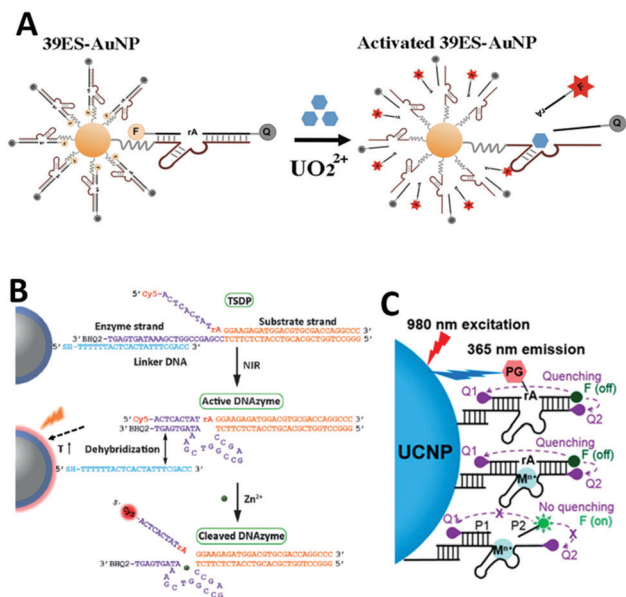
Fig. 14   (A) Design of a fluorescent DNAzyme immobilized onto AuNPs as a selective probe of uranyl inside live cells. Reprinted with permission from ref. 180. Copyright (2013) American Chemical Society. (B) Near-infrared (NIR) photothermally activated DNAzyme using a three-stranded DNA-zyme precursor (TSDP). Reprinted with permission from ref. 181. Copyright (2017) Wiley-VCH. (C) Upconversion nanoparticle (UCNP)-based photo-activatable DNAzymes. Reprinted with permission from ref. 184. Copyright (2018) American Chemical Society.

prevents DNAzyme activity. The TSDP is conjugated onto AuNS *via* Au–S chemistry. NIR illumination causes an increase in temperature which results in dehybridization of the TSDP to release the active DNAzyme. The active DNAzyme then catalyzes the metal ion-dependent cleavage to release the cleaved product that contains a fluorophore. Using this construct, the detection of Zn^{2+} in living HeLa cells has been demonstrated. The method has expanded the versatility of DNAzymes for detecting metal ions in biological systems with spatiotemporal control. Alternatively, the use of upconversion nanoparticles (UCNPs) also realized this goal as they absorb long-wavelength NIR light to generate short-wavelength photons, which is beneficial for *in vivo* studies due to the low autofluorescence background, negligible photodamage and remarkable penetration depth.[182,183] Taking advantage of this feature, the limitation of irradiating living cells with harmful UV light can be avoided when conjugating the previously reported UV light sensitive photocaged DNAzyme at the inter-faces of UCNPs. The deep tissue penetrating NIR 980 nm light is locally converted to a 365 nm emission, which further decages the inactive photocaged DNAzyme. This integrated system helps to monitor the dynamic distribution of zinc in cells and zebrafish (Fig. 14C).[184]

Similarly, an activatable aptamer nanodevice engineered at the interface of UCNPs was demonstrated.[185] UV-light activatable ATP aptamers were functionalized onto UCNPs, which worked as a signal transducer to operate the nanodevice in response to irradiated NIR light. The target-binding ability of the ATP aptamer was initially inhibited by hybridizing with a

UV photocleavable group (PC) incorporated locker strand. A pair of FRET donor and acceptor molecules were modified at each terminus of the DNA duplex, resulting in negligible background fluorescence. Under NIR irradiation, the UCNP converted the NIR light into UV light to photolyze the PC group. The resulting short oligonucleotide with low binding affinity disassociated from the aptamer, leading to ATP binding along with fluorescence signal recovery.

4.3.2   Pore opening for bioimaging and drug release based on DNAzyme and aptamer. RNA-cleaving DNAzymes are another set of ideal candidates for pore caging of porous nanoparticles. As a proof of concept, thiolated substrate strands of DNAzymes were immobilized on the interface of MSNs using a crosslinker, and encapsulated molecules were caged in the pores by hybridizing with enzyme strands. DNAzymes were cleaved and molecules released in the presence of specific metal ions.[186] Since the catalytic activity of DNAzymes varied as a function of pH, a pH-controlled release platform was constructed by choosing Mg^{2+} and UO_2^{2+} DNAzymes.[187]

At pH 5.2, UO_2^{2+} DNAzyme caged molecules were released, whereas at pH 7.2, Mg^{2+} DNAzyme caged molecules were released. More interestingly, the trapped molecules in the engineered MSNs, caged by DNAzymes, reacted with each other to cause a programmed synthesis.[188] Similarly, DNAzymes can be used to engineer the interface of MOFs for drug release.[189]

Porous nanoparticles engineered by structure switching aptamers have been endowed with specific targeting capability realizing a series of biosensing and therapeutic applications. For example, the VEGF–AS1411 aptamer containing duplex DNA was reported to cage drug molecules in the pores of Zr^{4+} MOFs *via* click chemistry (Fig. 15A). As indicated by the confocal images in Fig. 15B, the exposed AS1411 aptamer targeted MDA-MB-231 cells instead of MCF-10A cells by specifically binding to membrane nucleolin. After cellular uptake, the over-expressed VEGF in cancerous cells was recognized by the aptamer, and the pore opened upon forming the VEGF/aptamer complex. The drug molecules were then released into the cell for further therapy.[190] Moreover, taking advantage of the strong coordination between Zr^{4+} and phosphate, DNA aptamers were engineered on the interface of MOFs for targeted imaging and photodynamic therapy.[70] The platform was found to be versatile and can be generalized to other aptamer and MOF nanomaterials.[191]

A comparison of responsive pore-opening strategies using DNA nanotechnology at nanoparticle interfaces is presented in Table 3. MSNs and MOFs are two commonly used porous nanoparticles for molecular caging. Based on a strand displacement reaction and RNA-cleaving DNAzyme/aptamer recognition, the responsive payload releasing platforms have found wide bioapplications in biosensing, targeted bioimaging and drug delivery. Making use of the strand displacement reaction, an endogenous nucleic acid biomarker was readily coupled with these platforms as a trigger to construct "on-demand" drug release systems. However, such a platform typically requires the elaborate design of several DNA strands, which is difficult to realize, especially for use in complex intracellular environments. A variety of *in vitro* selected DNAzymes and aptamers are now
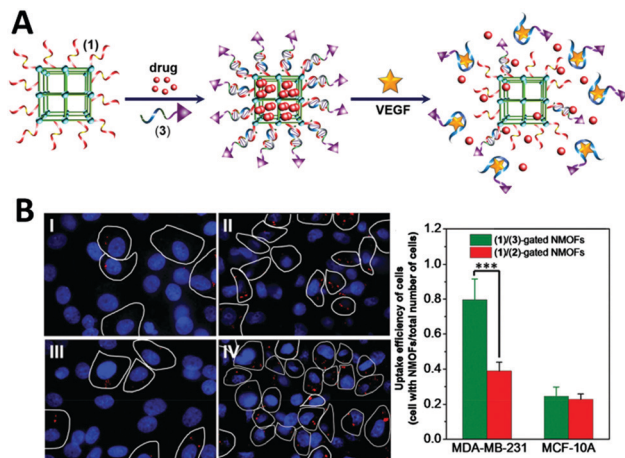
Fig. 15 (A) Schematic of the loading and release of doxorubicin from NMOFs gated with (1)/(3) nucleic acid locks, where (3) includes the caged VEGF aptamer conjugated to the AS1411 anti-nucleolin aptamer as the targeting probe. (B) Left: Confocal images corresponding to the uptake of the different doxorubicin-loaded NMOFs by MCF-10A breast cells (Panel I and Panel III, Panel I: without conjugation of the AS1411 aptamer; Panel III: with conjugation of the AS1411 aptamer) and MDA-MB-231 breast cancer cells (Panel II and Panel IV, Panel II: without conjugation of the AS1411 aptamer; Panel IV: with conjugation of the AS1411 aptamer); right: uptake efficiency of different samples. All reprinted with permission from ref. 190. Copyright (2018) Royal Society of Chemistry.

available to cage the porous nanoparticles for targeted imaging and drug release applications. However, the *in vivo* catalytic/targeting capability of DNAzymes/aptamers needs to be further studied and optimized to ensure the development of efficient biomedical applications.

DNA nanotechnology has provided useful tools to direct the construction of nanostructures and modify nanoparticle surface properties, offering more opportunities for wider bioapplications. Owing to the remarkable physical and chemical properties of numerous nanoparticles, they have been widely used as multifunctional carriers to construct diverse activatable platforms for biosensing, bioimaging and biomedical applications.

5. Bioapplications of DNA nanotechnology at "soft" interfaces

The "soft" interfaces here mainly refer to DNA origami and cell membranes. Compared with flat and nanoparticle interfaces, DNA origami interfaces have a number of intrinsic merits, including site addressability, versatile shapes, and programmable and ordered properties encoded in nucleotide sequences, and are recognized as a perfect platform for the assembly of multicomponent nanostructures. Double-helical DNA nanostructures provide unique binding sites with a regular spacing of approximately 7 nm (21 base pairs) along the helix and approximately 3 nm perpendicular to the helical axis.[192] This feature makes it easy and straightforward to precisely position nanocomponents at specific sites, highlighting the potential utility of DNA origami in guiding the design of DNA nanodevices. The localization of dynamic DNA reactions at precisely defined DNA origami interfaces should increase the local concentration of reactants and accelerate the reaction, which is beneficial for improved performance.[193] In addition, numerous molecules covering the cell membrane play an utmost important role in interactions between cells and the extracellular environment. DNA nanotechnology enabled strategies can monitor the dynamic interactions and help investigate biological events. Inspiring and representative examples will be presented below to show the potential applications of DNA nanotechnology at the cell membrane.

In this section, since most studies have combined structural and functional DNA nanotechnology with dynamic DNA nanotechnology, we summarize bioapplications based on the soft interface type instead of the branches of DNA nanotechnology.

5.1 Bioapplications of DNA nanotechnology at the interface of DNA origami

Multiple staple strands that constitute a DNA origami structure provide specific site addressability with high precision. Additionally, extended staple stands are available for anchoring various nanospecies, including DNA strands, enzymes and nanoparticles, offering an opportunity to construct multiple-component integrated interfaces. These elaborate engineering interfaces enable a wide range of applications that will be presented below.

5.1.1 Kinetic study of localized dynamic DNA reactions. Localized dynamic DNA reactions that take place at the interfaces of DNA origami are expected to be more efficient than in aqueous solution because of the increased local concentration of reactants.[194–196] Conceivably, however, the distance between strands involved in the reaction process plays a vital role. To study the distance effect, Teichmann *et al.* prepared a 90 nm × 65 nm rectangular DNA origami substrate, and the robustness of basic two-stage DNA strand displacement reactions at the DNA origami interface was thoroughly studied.[197] As shown in Fig. 16A, two consecutive gates were hybridized to the extension staple strands with varying distances of 3, 6, 9 and 12 full helical turns (nominally 10.5, 21.5, 32 and 42.5 nm) with the red dot indicating Gate 1 and the blue dot representing Gate 2. In the presence of input I, signal S at Gate 1 would be replaced

Table 3 A comparison of responsive pore opening strategies using DNA nanotechnology at the nanoparticle interface

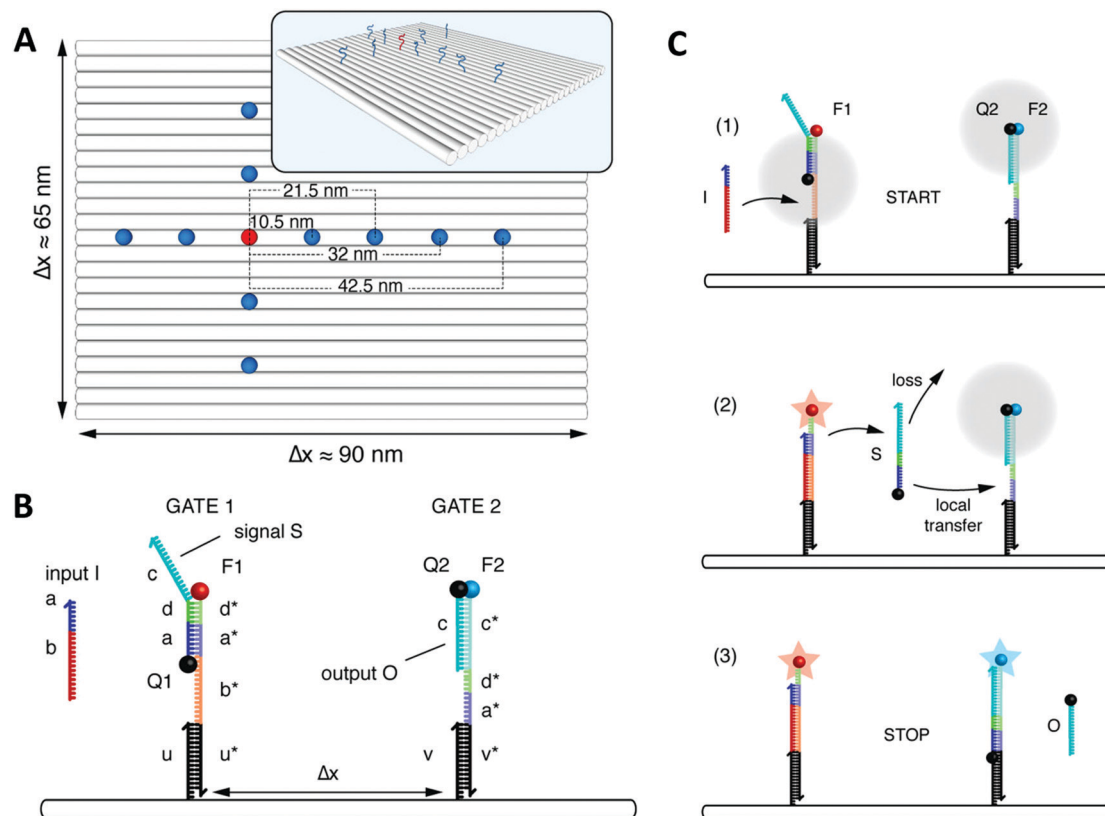| Nanoparticle species	Pore opening strategy	Bioapplications	Ref.
MSNs	Strand displacement reactions	"On-demand" drug delivery and biosensing	159 and 160
	RNA-cleaving DNAzymes	Molecular release and programmed synthesis	167–169
MOFs	RNA-cleaving DNAzymes	Drug delivery	170
	Aptamers	Targeted imaging and cancer therapy	70, 171 and 172

Fig. 16 (A) Two-stage DNA strand displacement (DSD) cascade engineered at the interface of rectangular DNA origami with different distances. (B) Detailed strands and domains involved in the DSD cascade shown in its initial state. (C) The DSD cascade reaction process. All reprinted with permission from ref. 197. Copyright (2014) American Chemical Society.

by a toehold-mediated branch migration reaction and subsequently hybridized to Gate 2 to release output O (Fig. 16B). The gate component was modified with a fluorophore and quencher to monitor the reaction process (Fig. 16C). A distance of 10.5 nm was found to be too close, and preparation of the defined initial state failed with a serious leakage reaction between the two gates. A system with a distance of 21.5 nm gave overall faster kinetics than the other longer distances. This result was due to a direct physical interaction of the gates at 21.5 nm, which allowed local strand transfer through an intermediary complex, whereas the distance increasing caused further diffusion of the released signal S from Gate 1 into the bulk solution. Thus, engineering an appropriate distance between consecutive dynamic DNA cascade reaction probes accelerates the reaction but also increases the robustness of the cascade through fast strand local transfer without diffusion into the bulk solution.

In contrast to the previous work, a study employing hairpin structures instead of typical ssDNA as the gate strand was conducted to investigate the kinetics of a more complicated localized HCR. A rectangle DNA origami, composed of 224 staple strands and a long scaffold M13mp18 (with a size of 70 nm × 85 nm), was utilized as the engineering interface. Faster reaction kinetics were observed when compared with that of the aqueous solution reaction.[198]

Constraining distances between DNA strands has been realized through rational engineering at the interfaces of the DNA origami. Such a design has provided faster reaction rates when compared with the bulk solution-based reaction, and thus laid the theoretical foundation for further related studies and bioapplications.

5.1.2 Engineering of highly controllable DNA nanodevices. DNA origami allows the interfacial engineering of advanced and controllable devices for wide applications,[199–201] and the DNA walker is the most frequently demonstrated. For example, at the interface of a 100 nm × 70 nm rectangular DNA origami, 17 tracks were equidistantly arranged with 6 nm gap sizes. Once the walker DNA hybridized with the track, cleavage by the nicking enzyme occurred in the track. Accordingly, a 6-nt toehold domain of the walker was exposed and walked to the next track. The consecutive and directional process of a single walker was monitored by high-speed, real-time AFM without dissociation.[202] In this study, the distance between tracks was carefully tuned by changing the specific position of the track on the DNA origami interface. The walking efficiency was also significantly affected by the distance between tracks.

Except for realizing simple walking operation in a predefined direction at the interface, multifunctional robots that walk as well as sort cargo or choose a pathway at a junction are highly desired. They are expected to be promising candidates to fulfill
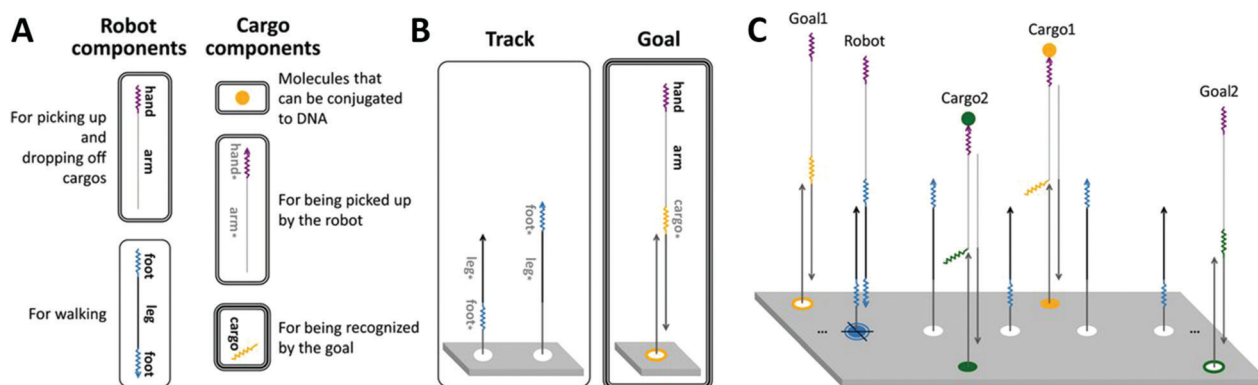
Fig. 17 (A) Composability of the three building blocks of a DNA robot. (B) Detailed components of track and goal. (C) Implementation for sorting multiple types of cargos. All reprinted with permission from ref. 49. Copyright (2017) American Association for the Advancement of Science.

sophisticated tasks, including autonomous chemical synthesis, programmable therapeutics and constructing stimuli-responsive molecular devices. The programmable properties of DNA origami interfaces enable the engineering of such a DNA robot.[49] Specifically, a cargo-sorting algorithm based on three modular building blocks (including that for random walk, for cargo pickup and for cargo drop-off) was developed to implement tasks (Fig. 17A). Two tracks were equidistantly engineered at the interface of the DNA origami in a checkerboard pattern with identical neighbors (Fig. 17B and C). The robot was able to randomly walk from any location to any neighboring location on the track without bias. As described in Fig. 17C, the robot that hybridized with the track at an arbitrary location was composed of two terminal foot domains and one leg domain. Random walking was enabled by the toehold-mediated branch migration reaction between two adjacent tracks. Further incorporation of an arm domain and a hand domain into the robot enabled cargo carrying and the drop-off task to be achieved through hybridization at a specific position. More interestingly, two types of cargos that were initially at unordered locations can be fully sorted to predefined destinations (Fig. 17C). Because sorting occurred at the interface of individual DNA origami, distinct tasks can be performed simultaneously by simply scaling up the system.

An increasing interest toward environmental stimuli responsive DNA origami interfaces has been witnessed in recent years. The engineering of DNA origami interfaces with environmentally responsive modalities is easy to realize by simply incorporating specific staple strands. For example, K^+ responsive G-quadruplex structures were used as fuel and input to engineer DNA origami cascade reaction interfaces. In the presence of K^+, the interfacial localized cascade circuits were inhibited because the G4 structure was formed, whereas removal of K^+ caused deformation of the G4 structure and the activation of the circuit for fluorescence signal amplification.[203] Similar to this example, photoresponsive[204] and electric-responsive[205] robots operating at DNA origami interfaces were also reported. Furthermore, robots engineered at the interface of a DNA origami have been reported to respond to intracellular molecules as a therapeutic in living cells, indicating their potential for *in vivo* bioapplications.[85,206]

5.1.3 Engineering the enzymatic cascade reaction. DNA origami interfaces offer a platform for the artificial colocalization and spatial organization of multiple enzymes at specific sites.[207] Systematically varying the distance of enzymes is straightforward using DNA origami scaffolds. The proximity of enzymes at certain nanometer scales on DNA origami scaffolds has been reported to enhance the cascade throughput. The glucose oxidase (GOx) and horseradish peroxidase (HRP) pair is the most frequently used model for related studies. For example, placing DNA-modified GOx and HRP next to each other with a distance of 10 nm at the DNA origami interface caused a more than 15-fold enhancement in activity compared with the free enzymes in solution.[208] Other pairs of enzymes that were engineered at the interface of DNA origami also showed the same activity enhancement behavior.[209,210] The strong activity enhancement is typically ascribed to the restricted diffusion of intermediates from one enzyme to the next enzyme in an enzyme cascade anchoring at the DNA origami interface, which is termed substrate channeling. However, the proposed mechanism is controversial because a GOx–HRP complex formed by a 2 nm crosslinker did not show an enhancement in activity similar to that of the DNA origami-based system. The authors concluded that the change in pH at the DNA origami interface contributed to the enhanced activity.[211] Additional related studies need to be performed to uncover the mechanism.

Rather than statically immobilizing multi-enzymes and swinging arms that facilitate substrate channeling with close proximity at the DNA origami interface,[209] the relative position of these species was reported to be regulated *via* light-driven dynamic DNA hybridization.[51] In this system, photoresponsive molecules of azobenzene (AZO) were incorporated into DNA. Light irradiation caused the *trans–cis* photoisomerization of AZO. The *trans* AZO enabled the hybridization of dsDNA, whereas *cis* AZO precluded the hybridization of dsDNA, realizing the photocontrol of hybridization/dehybridization of dsDNA. As shown in Fig. 18A, an AZO modified anchor was arranged on a DNA origami scaffold to selectively capture and release the AZO modified swing arm that held a cofactor. The swing arm was a Holiday Junction (HJ) structure and was positioned near two enzymes to facilitate substrate channeling. As depicted in
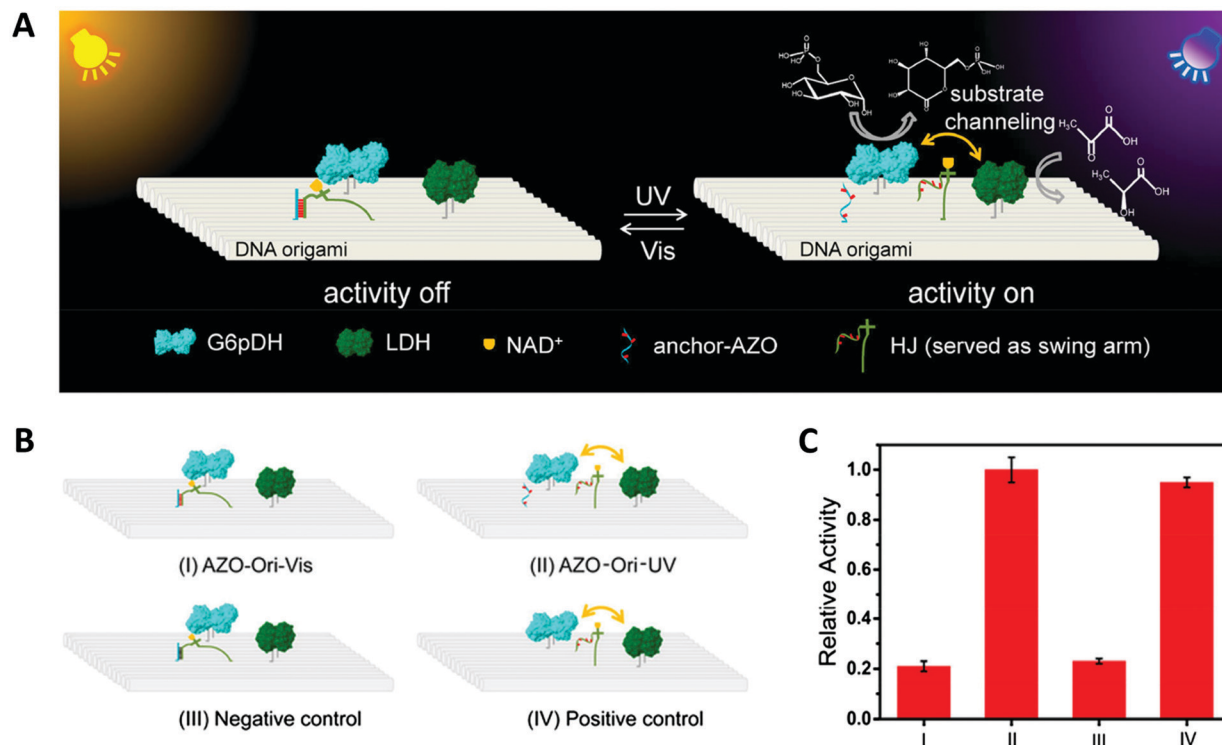
Fig. 18 (A) G6pDH–LDH enzyme cascade and NAD⁺–HJ swing arm assembly on the DNA origami scaffold. Schematic (B) and relative activities (C) of the four states of the enzyme cascade/DNA origami assembly. All reprinted with permission from ref. 51. Copyright (2018) American Chemical Society.

Fig. 18B, under visible light irradiation, the AZO-modified arm of the HJ was captured by the anchor, leading to the cofactor being located distal from the enzyme cascade. In contrast, UV light triggered the dehybridization of the AZO modified arm of the HJ with anchor and the free HJ returned to its initial position, which accelerated the relative catalytic activity by 5-fold (Fig. 18C).

5.1.4 Interrogating protein–ligand interactions. Protein–ligand interactions can be classified into several groups, including interactions of proteins with other proteins, peptides, nucleic acids as well as small molecules, antigen–antibody interactions, enzyme–inhibitor interactions and enzyme–substrate catalytic interactions. An in-depth understanding of the interactions between proteins and their target ligands plays an important role in understanding biology at the molecular level. Moreover, the detailed study of protein–ligand interactions also aids drug discovery platforms.

2D DNA origami nanostructures were used as a programmable nanosized substrate to construct pharmacophore nanoarrays for the discovery of small molecule protein inhibitors.[212] Specifically, a triangular DNA origami nanostructure with a 120 nm edge was synthesized. The model pharmacophores were attached at specific positions of the staple strands. The protein–pharmacophore interaction was quantitated by varying the pharmacophore number and distances between pharmacophores. Compared with microarray techniques, the size of the DNA origami-based nanoarray was reduced by several orders of magnitude, enabling the identification of protein–ligand interactions from weak

binders at a single-molecule level using AFM. Similarly, DNA origami was used as a pattern template for the arrangement of antigens, and the optimal distance between antigens for the binding of an antibody was studied. Varying the distances between antigens from 3 to 17 nm demonstrated that the strongest binding was obtained at approximately 16 nm.[213]

In addition to serving as flat templates for the precise arrangement of ligands, DNA origami nanocontainers or nano-capsules are powerful tools for protein caging.[214] For example, Sprengel and coworkers reported the selective encapsulation of a protein in a DNA origami cavity.[215] The inner side of the DNA origami nanocontainer was preattached with protein binding ligands at selected positions for further encapsulation *via* supramolecular interactions. One-to-one stoichiometry of protein and nanocontainer recognition was realized. Of note, binding of the protein to the container seemed to be permanent even after the removal of the ligands.

5.1.5 Engineering plasmonic nanoantennas for biosensing. Parallel to positioning proteins or ligands as mentioned above, nanoparticles can also be attached at the interface of a DNA origami molecular breadboard for nanophotonics and plasmonics.[216,217] Either fluorescent or other signal molecules were positioned in the near-field of plasmonic metallic nano-particles as nanoantennas with nanometric accuracy for biosensing applications. It was reported that the fluorescence signal at the nanoantenna hotspot between two nanoparticles was significantly enhanced. Specifically, two 100 nm gold nanoparticles were attached to the DNA origami pillar with

interparticle distances of 23 nm, and a fluorescent dye was attached to the central bundle of the pillar between two gold nanoparticles, and over 100-fold fluorescence enhancement was observed.[218] In a follow-up study, through optimization of the nanoconstruct robustness and the interparticle distance, the fluorescence enhancement was increased to 5000-fold, and single-molecule detection was demonstrated at a concentration of 25 μM.[219] Using a similar principle, Zika virus nucleic acid detection was performed without any signal amplification.[220] By immobilizing alkyne group modified streptavidin in the gap of two silver nanoparticles that were arranged at the interface of the DNA origami nanostructure, the SERS signal of a single streptavidin molecule was detected, paving the way for SERS study of complex biomolecules at the single-molecular level.[221]

All these successful examples support the concept that DNA origami interfaces are powerful and convenient platforms for the precise arrangement of oligonucleotides, enzymes, proteins and nanoparticles with high reproducibility, which is an important property for future bioapplications. More interestingly, by further combining the top-down micropatterning of solid surfaces with ligand modified DNA origami nanostructures, a series of examples for controlling and interrogating cellular responses have been successfully demonstrated.[222–224]

5.2 Bioapplications of DNA nanotechnology at the interface of the cell membrane

The cell membrane is composed of an assembly of lipids, proteins and carbohydrates, and characterizing this bioactive interface is of particular interest in the study of cell behavior. Cells interact with their surrounding environment through a variety of membrane proteins, which are usually recognized as vital biomarkers for disease diagnostics.[225–227] Cell membrane engineering methodologies that are enabled by DNA nanotechnology to disclose protein levels have garnered attention recently. For example, the overexpressed human epidermal growth factor receptor-2 (HER2) at the surface of breast cancer cells was revealed by this means. HER2 simultaneously bound to two antibodies that were conjugated to two DNA probes. The proximity of the two DNA probes triggered a toehold mediated strand displacement reaction on the cell membrane, leading to fluorescence recovery, designating the presence of HER2.[228] Similarly, the proximity mechanism was employed to engineer cell membranes to study the formation of the HER2:HER2 homodimer and the HER2:HER3 heterodimer,[229] and visualize the dimerization of the Met receptor.[230]

The aforementioned individual protein biomarker identification approaches cannot be employed to differentiate heterogeneity among cancer cell subtypes,[231] which is an obstacle for accurate diagnosis. In response to this problem, Peng et al. proposed a bispecific recognition strategy based on a 3D DNA AND logic gate nanomachine that was engineered at the interface of the cell membrane.[232] The 3D DNA logic gate is a triangular prism (TP) with overhangs at three vertices. The overhangs are two blocked aptamers and a fluorescent signal reporter consisting of a computing component. Only in the presence of human acute lymphoblastic leukemia cells (CCRF-CEM) could the

sgc8c (binding with tyrosine-protein kinase-like 7) and sgc4f aptamers (unidentified target) bind to the cells and release the blocking strand simultaneously to execute a strand displacement reaction-based logic gate operation at the cell membrane. The output signal was identified using confocal microscopy. In contrast, Romas cells did not show any visible fluorescence, demonstrating the possibility of precisely differentiating cancer cell subtypes using DNA nanotechnology.

Real-time monitoring of changes in the cellular environment *via* cell membrane engineering probes would be a valuable approach to understand the underlying mechanisms of cell metabolism and signaling. In this context, a diacyllipid-DNAzyme probe at the cell membrane interface was designed to monitor exogenous and cell extruded metal ions (Fig. 19A).[233] The probes were attached to the cell membrane with high efficiency *via* hydrophobic interactions between a lipophilic C18 hydrocarbon tail and the phospholipid bilayer, as indicated by the red fluorescence around the cell membrane (Fig. 19C). Taking advantage of the high selectivity and specificity of DNAzymes, the probes can respond to 20 mM Mg^{2+}. Significant fluorescence enhancement was clearly observed due to the separation of the quencher and fluorophore modified on the DNA strands caused by site cleavage (Fig. 19B). However, this cell membrane probe is nonreversible and loses sensing ability once cleaved by
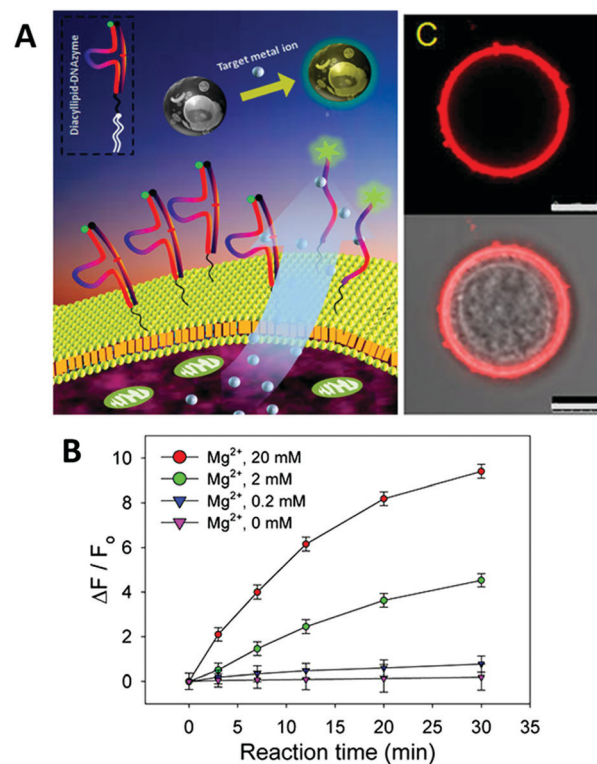

Fig. 19 (A) Schematic of the diacyllipid-DNAzyme probe at the cell membrane interface for real-time monitoring of metal ions. (B) Flow cytometry result of kinetics study for CEM cells incubated with the diacyllipid-DNAzyme probe and then treated with Mg^{2+} of different concentrations. (C) Confocal images of CEM cells incubated with diacyllipid-DNA-TAMRA. All reprinted with permission from ref. 233. Copyright (2014) American Chemical Society.

encountering metal ions, and a long-lasting sensing capacity therefore remains a challenge.

DNA nanotechnology enabled engineering at the interface of cell membranes can be used to organize receptors into nanoscale clusters, thereby manipulating cell behavior and controlling specific functions. For example, Zhang *et al.* presented a DNA nanospring-based method to control the distance between integrin on the cell membrane.[234] The DNA nanospring was synthesized by rolling circle amplification with the help of a circular DNA template. Multiple RGD (Arg-Gly-Asp) molecules were conjugated to the nanospring in advance through DNA hybridization, and these molecules helped the nanospring to bind to the cell due to their affinity to integrin on the cell membrane. The declustering of integrin was triggered by adding an auxiliary strand (cDNA1) to open the intrinsic encoding hairpin structures, resulting in the activation of PI3K/Rac1 signaling and the generation of protrusions for cell morphology (Fig. 20). The clustering of integrin was easily recovered by incubating with a competing strand (cDNA2). Strand displacement reaction took place to displace cDNA1 from the nanospring template, leading to normal cell morphology. This report demonstrated that the rational design of DNA nanotechnology at the interface of cell membranes modulates the morphology and gene expression of the manipulated cells.

More interestingly, a chemically induced dimerization (D-CID) of cell receptors mediated by DNA was proposed to activate signaling pathways and further control cell behavior.[235] C-Met, a receptor tyrosine kinase for the hepatic growth factor on cell membranes, was used as a model. Two subunits were linked to the extracellular side of c-Met by a specific binding aptamer. One subunit was partially caged by an ATP aptamer, thus prohibiting the hybridization of two subunits. Subsequent introduction of ATP uncaged the toehold domain of this subunit and triggered a strand displacement reaction, causing the two subunits to come into close proximity. As a result, heterodimerization of two c-Met proteins was observed and autophosphorylation occurred. The downstream activation of actin lamellipodium was also demonstrated to increase the mobility of cells.
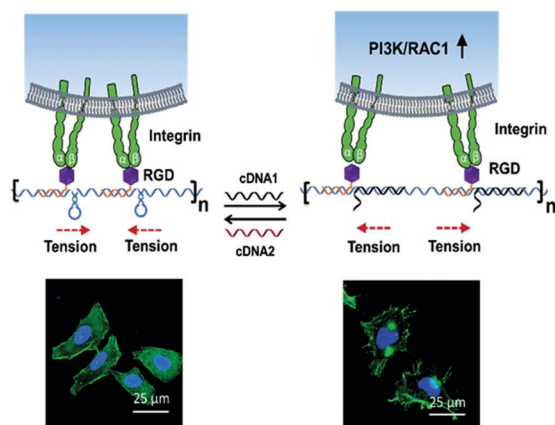

Fig. 20 DNA nanospring-triggered integrin clustering and declustering is able to regulate intracellular signalling pathways and cell morphology. Reprinted with permission from ref. 234. Copyright (2017) Royal Society of Chemistry.

A polarization ratio of 63% was observed under ATP gradient treatment, illustrating customized chemotaxis of the DNA nanotechnology engineered cells.

6. Conclusions and perspectives

The past decade has witnessed the development of a range of bioapplications enabled by DNA nanotechnology at the solid–liquid interface, including biosensing, bioimaging, and *in vitro* and *in vivo* biomedicine. From these studies, we have learned that interfaces play the following main roles: the interface provides a constrained platform to immobilize ssDNA, dsDNA and 3D DNA nanostructures, facilitating DNA hybridization and DNA walker/motor system operation, and it can be tailored to improve biosensing performance. Localization of the DNA reaction at a variety of interfaces is similar to compartmentalization in biology, which is enabled by membranes. Distinct local functions are performed in parallel without losing high efficiency.[236] In addition, the nanoparticles used to immobilize DNA always possess specific optical, electrical, colorimetric, or photothermal properties, endowing excellent physical and chemical properties to the DNA nanoparticle systems for a wider range of bioapplications. The interfaces also act as carriers to deliver DNA-based systems into cells and organisms, opening new avenues for *in vivo* bioapplications of DNA nanotechnology. Despite all these examples of progress, we have identified some challenges currently faced by the field, and the underlying future prospects are provided below.

First, continuing research on kinetics is required to improve DNA nanostructure interfacial systems and expand the scope of bioapplications. Although studies (as described above) have shown improved reaction rates for all kinds of interfaces enabled by DNA nanotechnology, the reaction species are limited to dynamic cascade reactions. Investigations on the kinetics of aptamer structure switching and RNA-cleaving DNAzymes at the solid–liquid interfaces should be encouraged. The influence of different interfaces on these functional molecules needs to be addressed to provide fundamental guidelines for more bioapplications. The rational engineering of sequences, for example by adding appropriate lengths of poly-oligonucleotides, is also necessary.

Second, the stability of DNA anchorage at interfaces is a significant challenge that needs to be overcome, especially in complex environments such as biological samples. Ultrastable interfaces enabled by DNA nanotechnology significantly contribute to the high signal-to-background ratio (S/N) in biosensing and bioimaging systems, as well as controlling the release behavior of molecules for biomedical applications. There are two levels of ultrastable interfaces enabled by DNA nanotechnology: (1) the conjugation of DNA to the surface should be sufficiently stable to avoid shedding from the surface. For example, the widely used Au–S bond is readily replaced by intracellular reductive molecules such as GSH. Recently, it was reported by the Tang group that the Se–Au bond is more stable under a reductive cellular environment, enabling more reliable bioapplication *in vivo*.[237] This issue has also

been addressed by embedding the DNA into the nanoparticles during the synthesis process using DNA as the template.[238–242] For example, the Lu group has demonstrated that DNA on gold nanoflowers using DNA encoded growth of nanoparticles is much more stable than the Au–S bond.[243] New conjugation chemistry that forms more stable linkages, such as click chemistry, is highly desired for use in interface engineering. (2) The surface should be sufficiently stable to not show any degradation during the bioapplication. For example, MOFs are easily decomposed in biological environments to nonspecifically release the caged molecules. High concentrations of divalent metal ions (10–20 mM Mg^{2+}) are necessary to stabilize DNA origami nanostructures, yet cells do not provide these extreme conditions, limiting their further use. To address these challenges, the preparation of more stable nanoparticles and DNA origami interfaces should be explored. For example, it was recently demonstrated that the amphiphilic polymer poly[isobutylene-*alt*-maleic anhydride]-*graft*-dodecyl (PMA) stabilized ZIF-8 exhibited excellent stability both in aqueous solution and in living cells compared with bare ZIF-8.[244] By choosing appropriate DNA origami superstructures and buffer components, the stability and structural integrity of DNA origami nanostructures can be maintained for at least two months even at a concentration of 10 μM Mg^{2+}.[245]

Third, reversibility is highly desired for all kinds of interfacial dynamic DNA machines. Most DNA machines engineered at interfaces rely on the burned-bridge mechanism; the tracks can be completely destroyed after one round of operation. In addition, the nanodevices are still very primitive and the current assembly lines can be used only once. Similar to their natural counterparts, reversible and reusable mechanisms are desired. One solution is to use external stimuli to reset the *in vivo* systems, such as pH, light, heat and electricity. For *in vitro* systems, except for those strategies mentioned above, different binding affinities of biotin and desthiobiotin toward streptavidin have been successfully demonstrated for reversible DNA origami interface construction.[246]

In the future, we are optimistic that bioapplications that utilize DNA nanotechnology at the solid–liquid interface will increase because of the versatile choices in interfaces and the ever-growing DNA nanotechnology toolbox, as well as our understanding of reaction kinetics. We believe it is time to move to the next stage of real-world applications. Recent studies of DNA nanotechnology operations were performed in zebrafish.[184,247] Nanoscale engineering of biological interfaces using DNA nanotechnology is anticipated to facilitate the future diagnosis and treatment of diseases, including cancer.

Conflicts of interest

There are no conflicts to declare.

Acknowledgements

References

1 N. C. Seeman and H. F. Sleiman, *Nat. Rev. Mater.*, 2017, **3**, 17068.

2 Y. Ke, C. Castro and J. H. Choi, *Annu. Rev. Biomed. Eng.*, 2018, **20**, 375–401.

3 R. Huang, N. He and Z. Li, *Biosens. Bioelectron.*, 2018, **109**, 27–34.

4 Q. Hu, H. Li, L. Wang, H. Gu and C. Fan, *Chem. Rev.*, 2019, **119**, 6459–6506.

5 C. Zhou, X. Duan and N. Liu, *Acc. Chem. Res.*, 2017, **50**, 2906–2914.

6 Z. Bing, W. Lihua, L. Jiang and F. Chunhai, *Chem. Rec.*, 2017, **17**, 1213–1230.

7 J. I. Cutler, E. Auyeung and C. A. Mirkin, *J. Am. Chem. Soc.*, 2012, **134**, 1376–1391.

8 R. Hong, G. Han, J. M. Fernández, B.-j. Kim, N. S. Forbes and V. M. Rotello, *J. Am. Chem. Soc.*, 2006, **128**, 1078–1079.

9 Z. Wu, G.-Q. Liu, X.-L. Yang and J.-H. Jiang, *J. Am. Chem. Soc.*, 2015, **137**, 6829–6836.

10 C. Sönnichsen, B. M. Reinhard, J. Liphardt and A. P. Alivisatos, *Nat. Biotechnol.*, 2005, **23**, 741–745.

11 M.-E. Kyriazi, D. Giust, A. H. El-Sagheer, P. M. Lackie, O. L. Muskens, T. Brown and A. G. Kanaras, *ACS Nano*, 2018, **12**, 3333–3340.

12 T. Torring, N. V. Voigt, J. Nangreave, H. Yan and K. V. Gothelf, *Chem. Soc. Rev.*, 2011, **40**, 5636–5646.

13 J. Li, A. A. Green, H. Yan and C. Fan, *Nat. Chem.*, 2017, **9**, 1056–1067.

14 Y. Lu and J. Liu, *Curr. Opin. Biotechnol.*, 2006, **17**, 580–588.

15 D. Y. Zhang and G. Seelig, *Nat. Chem.*, 2011, **3**, 103–113.

16 P. Chidchob and H. F. Sleiman, *Curr. Opin. Chem. Biol.*, 2018, **46**, 63–70.

17 N. C. Seeman, *J. Theor. Biol.*, 1982, **99**, 237–247.

18 C. Mao, *PLoS Biol.*, 2004, **2**, e431.

19 E. Winfree, F. Liu, L. A. Wenzler and N. C. Seeman, *Nature*, 1998, **394**, 539–544.

20 Y. He, Y. Chen, H. Liu, A. E. Ribbe and C. Mao, *J. Am. Chem. Soc.*, 2005, **127**, 12202–12203.

21 B. Wei, M. Dai and P. Yin, *Nature*, 2012, **485**, 623–626.

22 Y. He, T. Ye, M. Su, C. Zhang, A. E. Ribbe, W. Jiang and C. Mao, *Nature*, 2008, **452**, 198–201.

23 C. Zhang, M. Su, Y. He, X. Zhao, P.-a. Fang, A. E. Ribbe, W. Jiang and C. Mao, *Proc. Natl. Acad. Sci. U. S. A.*, 2008, **105**, 10665–10669.

24 S. M. Douglas, A. H. Marblestone, S. Teerapittayanon, A. Vazquez, G. M. Church and W. M. Shih, *Nucleic Acids Res.*, 2009, **37**, 5001–5006.

25 F. Zhang, J. Nangreave, Y. Liu and H. Yan, *J. Am. Chem. Soc.*, 2014, **136**, 11198–11211.

26 P. S. Weiss, *ACS Nano*, 2008, **2**, 1089–1096.

27 J. H. Chen, M. E. A. Churchill, T. D. Tullius, N. R. Kallenbach and N. C. Seeman, *Biochemistry*, 1988, **27**, 6032–6038.

28 T. H. LaBean, H. Yan, J. Kopatsch, F. Liu, E. Winfree, J. H. Reif and N. C. Seeman, *J. Am. Chem. Soc.*, 2000, **122**, 1848–1860.

29 P. W. K. Rothemund, A. Ekani-Nkodo, N. Papadakis, A. Kumar, D. K. Fygenson and E. Winfree, *J. Am. Chem. Soc.*, 2004, **126**, 16344–16352.

30 D. Liu, S. H. Park, J. H. Reif and T. H. LaBean, *Proc. Natl. Acad. Sci. U. S. A.*, 2004, **101**, 717–722.

31 W. M. Shih, J. D. Quispe and G. F. Joyce, *Nature*, 2004, **427**, 618–621.

32 R. P. Goodman, I. A. T. Schaap, C. F. Tardin, C. M. Erben, R. M. Berry, C. F. Schmidt and A. J. Turberfield, *Science*, 2005, **310**, 1661–1665.

33 N. Xie, S. Liu, X. Yang, X. He, J. Huang and K. Wang, *Analyst*, 2017, **142**, 3322–3332.

34 Y. Zhang, W. Ma, Y. Zhu, S. Shi, Q. Li, C. Mao, D. Zhao, Y. Zhan, J. Shi, W. Li, L. Wang, C. Fan and Y. Lin, *Nano Lett.*, 2018, **18**, 5652–5659.

35 H. B. D. Thai, F. Levi-Acobas, S.-Y. Yum, G. Jang, M. Hollenstein and D.-R. Ahn, *Chem. Commun.*, 2018, **54**, 9410–9413.

36 P. W. K. Rothemund, *Nature*, 2006, **440**, 297–302.

37 G. Grossi, M. Dalgaard Ebbesen Jepsen, J. Kjems and E. S. Andersen, *Nat. Commun.*, 2017, **8**, 992.

38 V. V. Thacker, L. O. Herrmann, D. O. Sigle, T. Zhang, T. Liedl, J. J. Baumberg and U. F. Keyser, *Nat. Commun.*, 2014, **5**, 3448.

39 S. Loescher, S. Groer and A. Walther, *Angew. Chem., Int. Ed.*, 2018, **57**, 10436–10448.

40 D. Han, X. Qi, C. Myhrvold, B. Wang, M. Dai, S. Jiang, M. Bates, Y. Liu, B. An, F. Zhang, H. Yan and P. Yin, *Science*, 2017, **358**, eaao2648.

41 D. Soloveichik, G. Seelig and E. Winfree, *Proc. Natl. Acad. Sci. U. S. A.*, 2010, **107**, 5393–5398.

42 D. Y. Zhang and E. Winfree, *J. Am. Chem. Soc.*, 2009, **131**, 17303–17314.

43 B. Yurke, A. J. Turberfield, A. P. Mills Jr, F. C. Simmel and J. L. Neumann, *Nature*, 2000, **406**, 605–608.

44 J.-S. Shin and N. A. Pierce, *J. Am. Chem. Soc.*, 2004, **126**, 10834–10835.

45 T.-G. Cha, J. Pan, H. Chen, J. Salgado, X. Li, C. Mao and J. H. Choi, *Nat. Nanotechnol.*, 2013, **9**, 39–43.

46 L. Qian and E. Winfree, *Science*, 2011, **332**, 1196–1201.

47 J. Pan, F. Li, T.-G. Cha, H. Chen and J. H. Choi, *Curr. Opin. Biotechnol.*, 2015, **34**, 56–64.

48 D. C. Khara, J. S. Schreck, T. E. Tomov, Y. Berger, T. E. Ouldridge, J. P. K. Doye and E. Nir, *Nucleic Acids Res.*, 2018, **46**, 1553–1561.

49 A. J. Thubagere, W. Li, R. F. Johnson, Z. Chen, S. Doroudi, Y. L. Lee, G. Izatt, S. Wittman, N. Srinivas, D. Woods, E. Winfree and L. Qian, *Science*, 2017, **357**, eaan6558.

50 Y. Amir, E. Ben-Ishay, D. Levner, S. Ittah, A. Abu-Horowitz and I. Bachelet, *Nat. Nanotechnol.*, 2014, **9**, 353–357.

51 Y. Chen, G. Ke, Y. Ma, Z. Zhu, M. Liu, Y. Liu, H. Yan and C. J. Yang, *J. Am. Chem. Soc.*, 2018, **140**, 8990–8996.

52 R. Peng, X. Zheng, Y. Lyu, L. Xu, X. Zhang, G. Ke, Q. Liu, C. You, S. Huan and W. Tan, *J. Am. Chem. Soc.*, 2018, **140**, 9793–9796.

53 L. He, D. Lu, H. Liang, S. Xie, X. Zhang, Q. Liu, Q. Yuan and W. Tan, *J. Am. Chem. Soc.*, 2018, **140**, 258–263.

54 R. M. Dirks and N. A. Pierce, *Proc. Natl. Acad. Sci. U. S. A.*, 2004, **101**, 15275–15278.

55 S. Bi, S. Yue and S. Zhang, *Chem. Soc. Rev.*, 2017, **46**, 4281–4298.

56 R. Lin, Q. Feng, P. Li, P. Zhou, R. Wang, Z. Liu, Z. Wang, X. Qi, N. Tang, F. Shao and M. Luo, *Nat. Methods*, 2018, **15**, 275–278.

57 Y. Jiang, B. Li, J. N. Milligan, S. Bhadra and A. D. Ellington, *J. Am. Chem. Soc.*, 2013, **135**, 7430–7433.

58 P. Yin, H. M. T. Choi, C. R. Calvert and N. A. Pierce, *Nature*, 2008, **451**, 318–322.

59 Z. Wu, H. Fan, N. S. R. Satyavolu, W. Wang, R. Lake, J.-H. Jiang and Y. Lu, *Angew. Chem., Int. Ed.*, 2017, **129**, 8847–8851.

60 A. P. K. K. Karunanayake Mudiyanselage, Q. Yu, M. A. Leon-Duque, B. Zhao, R. Wu and M. You, *J. Am. Chem. Soc.*, 2018, **140**, 8739–8745.

61 S. Yue, X. Song, W. Song and S. Bi, *Chem. Sci.*, 2019, **10**, 1651–1658.

62 J. Y. Kishi, T. E. Schaus, N. Gopalkrishnan, F. Xuan and P. Yin, *Nat. Chem.*, 2017, **10**, 155–164.

63 R. P. Chen, D. Blackstock, Q. Sun and W. Chen, *Nat. Chem.*, 2018, **10**, 474–481.

64 J. Hemphill and A. Deiters, *J. Am. Chem. Soc.*, 2013, **135**, 10512–10518.

65 W. Wang, S. Huang, J. Li, K. Rui, S. Bi, J.-R. Zhang and J.-J. Zhu, *Chem. Sci.*, 2017, **8**, 174–180.

66 T. Lin, J. Yan, L. L. Ong, J. Robaszewski, H. D. Lu, Y. Mi, P. Yin and B. Wei, *Nano Lett.*, 2018, **18**, 4791–4795.

67 H.-M. Meng, H. Liu, H. Kuai, R. Peng, L. Mo and X.-B. Zhang, *Chem. Soc. Rev.*, 2016, **45**, 2583–2602.

68 S. Dehghani, R. Nosrati, M. Yousefi, A. Nezami, F. Soltani, S. M. Taghdisi, K. Abnous, M. Alibolandi and M. Ramezani, *Biosens. Bioelectron.*, 2018, **110**, 23–37.

69 G. Liu, J. Li, D.-Q. Feng, J.-J. Zhu and W. Wang, *Anal. Chem.*, 2017, **89**, 1002–1008.

70 Y. Liu, W. Hou, L. Xia, C. Cui, S. Wan, Y. Jiang, Y. Yang, Q. Wu, L. Qiu and W. Tan, *Chem. Sci.*, 2018, **9**, 7505–7509.

71 J. Zhou and J. Rossi, *Nat. Rev. Drug Discovery*, 2016, **16**, 181–202.

72 H. Liu, J. Mai, J. Shen, J. Wolfram, Z. Li, G. Zhang, R. Xu, Y. Li, C. Mu, Y. Zu, X. Li, G. L. Lokesh, V. Thiviyanathan, D. E. Volk, D. G. Gorenstein, M. Ferrari, Z. Hu and H. Shen, *Theranostics*, 2018, **8**, 31–44.

73 Y. Jiang, X. Pan, J. Chang, W. Niu, W. Hou, H. Kuai, Z. Zhao, J. Liu, M. Wang and W. Tan, *J. Am. Chem. Soc.*, 2018, **140**, 6780–6784.

74 J. Zhang, L. P. Smaga, N. S. R. Satyavolu, J. Chan and Y. Lu, *J. Am. Chem. Soc.*, 2017, **139**, 17225–17228.

75 Y. Li and R. R. Breaker, *Curr. Opin. Struct. Biol.*, 1999, **9**, 315–323.

76 R. R. Breaker and G. F. Joyce, *Chem. Biol.*, 1994, **1**, 223.

77 J. Li and Y. Lu, *J. Am. Chem. Soc.*, 2000, **122**, 10466–10467.

78 F. Szurdoki, D. Ren and D. R. Walt, *Anal. Chem.*, 2000, **72**, 5250–5257.

79 C. E. McGhee, K. Y. Loh and Y. Lu, *Curr. Opin. Biotechnol.*, 2017, **45**, 191–201.

80 K. Hwang, P. Wu, T. Kim, L. Lei, S. Tian, Y. Wang and Y. Lu, *Angew. Chem., Int. Ed.*, 2014, **53**, 13798–13802.

81 S.-F. Torabi, P. Wu, C. E. McGhee, L. Chen, K. Hwang, N. Zheng, J. Cheng and Y. Lu, *Proc. Natl. Acad. Sci. U. S. A.*, 2015, **112**, 5903–5908.

82 H. Peng, X.-F. Li, H. Zhang and X. C. Le, *Nat. Commun.*, 2017, **8**, 14378.

83 J. Ding, W. Zhou and J. Liu, *Theranostics*, 2017, **7**, 1010–1025.

84 F. Chen, M. Bai, K. Cao, Y. Zhao, X. Cao, J. Wei, N. Wu, J. Li, L. Wang, C. Fan and Y. Zhao, *ACS Nano*, 2017, **11**, 11908–11914.

85 S. Li, Q. Jiang, S. Liu, Y. Zhang, Y. Tian, C. Song, J. Wang, Y. Zou, G. J. Anderson, J.-Y. Han, Y. Chang, Y. Liu, C. Zhang, L. Chen, G. Zhou, G. Nie, H. Yan, B. Ding and Y. Zhao, *Nat. Biotechnol.*, 2018, **36**, 258–264.

86 Y.-M. Wang, Z. Wu, S.-J. Liu and X. Chu, *Anal. Chem.*, 2015, **87**, 6470–6474.

87 E. E. Ferapontova, *Annu. Rev. Anal. Chem.*, 2018, **11**, 197–218.

88 H. Pei, X. Zuo, D. Pan, J. Shi, Q. Huang and C. Fan, *NPG Asia Mater.*, 2013, **5**, e51.

89 H. Pei, N. Lu, Y. Wen, S. Song, Y. Liu, H. Yan and C. Fan, *Adv. Mater.*, 2010, **22**, 4754–4758.

90 M. Lin, J. Wang, G. Zhou, J. Wang, N. Wu, J. Lu, J. Gao, X. Chen, J. Shi, X. Zuo and C. Fan, *Angew. Chem., Int. Ed.*, 2015, **54**, 2151–2155.

91 H. Pei, Y. Wan, J. Li, H. Hu, Y. Su, Q. Huang and C. Fan, *Chem. Commun.*, 2011, **47**, 6254–6256.

92 Y. Wen, H. Pei, Y. Wan, Y. Su, Q. Huang, S. Song and C. Fan, *Anal. Chem.*, 2011, **83**, 7418–7423.

93 Y. Wen, H. Pei, Y. Shen, J. Xi, M. Lin, N. Lu, X. Shen, J. Li and C. Fan, *Sci. Rep.*, 2012, **2**, 867.

94 Z. Ge, M. Lin, P. Wang, H. Pei, J. Yan, J. Shi, Q. Huang, D. He, C. Fan and X. Zuo, *Anal. Chem.*, 2014, **86**, 2124–2130.

95 M. Lin, Y. Wen, L. Li, H. Pei, G. Liu, H. Song, X. Zuo, C. Fan and Q. Huang, *Anal. Chem.*, 2014, **86**, 2285–2288.

96 P. Miao, B. Wang, F. Meng, J. Yin and Y. Tang, *Bioconjugate Chem.*, 2015, **26**, 602–607.

97 X. Chen, G. Zhou, P. Song, J. Wang, J. Gao, J. Lu, C. Fan and X. Zuo, *Anal. Chem.*, 2014, **86**, 7337–7342.

98 G. Zhou, M. Lin, P. Song, X. Chen, J. Chao, L. Wang, Q. Huang, W. Huang, C. Fan and X. Zuo, *Anal. Chem.*, 2014, **86**, 7843–7848.

99 S. Dong, R. Zhao, J. Zhu, X. Lu, Y. Li, S. Qiu, L. Jia, X. Jiao, S. Song, C. Fan, R. Hao and H. Song, *ACS Appl. Mater. Interfaces*, 2015, **7**, 8834–8842.

100 M. Giovanni, I. Setyawati Magdiel, Y. Tay Chor, H. Qian, S. Kuan Win and T. Leong David, *Adv. Funct. Mater.*, 2015, **25**, 3840–3846.

101 J. Wang, M. C. Leong, E. Z. W. Leong, W. S. Kuan and D. T. Leong, *Anal. Chem.*, 2017, **89**, 6900–6906.

102 Y. Li, Y. Wen, L. Wang, W. Liang, L. Xu, S. Ren, Z. Zou, X. Zuo, C. Fan, Q. Huang, G. Liu and N. Jia, *Biosens. Bioelectron.*, 2015, **67**, 364–369.

103 M. Lin, P. Song, G. Zhou, X. Zuo, A. Aldalbahi, X. Lou, J. Shi and C. Fan, *Nat. Protoc.*, 2016, **11**, 1244–1263.

104 Q.-M. Feng, Z. Zhou, M.-X. Li, W. Zhao, J.-J. Xu and H.-Y. Chen, *Biosens. Bioelectron.*, 2017, **90**, 251–257.

105 Q.-M. Feng, Y.-H. Guo, J.-J. Xu and H.-Y. Chen, *ACS Appl. Mater. Interfaces*, 2017, **9**, 17637–17644.

106 Q.-M. Feng, Y.-H. Guo, J.-J. Xu and H.-Y. Chen, *Biosens. Bioelectron.*, 2018, **100**, 571–576.

107 C. Li, X. Hu, J. Lu, X. Mao, Y. Xiang, Y. Shu and G. Li, *Chem. Sci.*, 2018, **9**, 979–984.

108 P. Zhang, J. Jiang, R. Yuan, Y. Zhuo and Y. Chai, *J. Am. Chem. Soc.*, 2018, **140**, 9361–9364.

109 D. Zhu, H. Pei, G. Yao, L. Wang, S. Su, J. Chao, L. Wang, A. Aldalbahi, S. Song, J. Shi, J. Hu, C. Fan and X. Zuo, *Adv. Mater.*, 2016, **28**, 6860–6865.

110 D. Daems, W. Pfeifer, I. Rutten, B. Saccà, D. Spasic and J. Lammertyn, *ACS Appl. Mater. Interfaces*, 2018, **10**, 23539–23547.

111 E. Pibiri, P. Holzmeister, B. Lalkens, G. P. Acuna and P. Tinnefeld, *Nano Lett.*, 2014, **14**, 3499–3503.

112 E. Torelli, M. Manzano, S. K. Srivastava and R. S. Marks, *Biosens. Bioelectron.*, 2018, **99**, 209–215.

113 A. Aghebat Rafat, T. Pirzer, M. B. Scheible, A. Kostina and F. C. Simmel, *Angew. Chem., Int. Ed.*, 2014, **53**, 7665–7668.

114 L. Liu, Y. Li, Y. Wang, J. Zheng and C. Mao, *ChemBioChem*, 2017, **18**, 2404–2407.

115 C. Kielar, S. Ramakrishnan, S. Fricke, G. Grundmeier and A. Keller, *ACS Appl. Mater. Interfaces*, 2018, **10**, 44844–44853.

116 S. Ramakrishnan, S. Subramaniam, A. F. Stewart, G. Grundmeier and A. Keller, *ACS Appl. Mater. Interfaces*, 2016, **8**, 31239–31247.

117 H. Aslan, A. Krissanaprasit, F. Besenbacher, K. V. Gothelf and M. Dong, *Nanoscale*, 2016, **8**, 15233–15240.

118 L. Liu, M. Zheng, Z. Li, Q. Li and C. Mao, *ACS Appl. Mater. Interfaces*, 2019, **11**, 13853.

119 M. Sajfutdinow, K. Uhlig, A. Prager, C. Schneider, B. Abel and D. M. Smith, *Nanoscale*, 2017, **9**, 15098–15106.

120 S. Hernández-Ainsa and U. F. Keyser, *Nanoscale*, 2014, **6**, 14121–14132.

121 N. A. W. Bell and U. F. Keyser, *FEBS Lett.*, 2014, **588**, 3564–3570.

122 N. A. W. Bell, C. R. Engst, M. Ablay, G. Divitini, C. Ducati, T. Liedl and U. F. Keyser, *Nano Lett.*, 2012, **12**, 512–517.

123 C. Plesa, A. N. Ananth, V. Linko, C. Gülcher, A. J. Katan, H. Dietz and C. Dekker, *ACS Nano*, 2014, **8**, 35–43.

124 S. Hernández-Ainsa, N. A. W. Bell, V. V. Thacker, K. Göpfrich, K. Misiunas, M. E. Fuentes-Perez, F. Moreno-Herrero and U. F. Keyser, *ACS Nano*, 2013, **7**, 6024–6030.

125 M. Langecker, V. Arnaut, T. G. Martin, J. List, S. Renner, M. Mayer, H. Dietz and F. C. Simmel, *Science*, 2012, **338**, 932–936.

126 J. R. Burns, K. Göpfrich, J. W. Wood, V. V. Thacker, E. Stulz, U. F. Keyser and S. Howorka, *Angew. Chem., Int. Ed.*, 2013, **52**, 12069–12072.

127 J. R. Burns, N. Al-Juffali, S. M. Janes and S. Howorka, *Angew. Chem., Int. Ed.*, 2014, **53**, 12466–12470.

128 J. R. Burns, A. Seifert, N. Fertig and S. Howorka, *Nat. Nanotechnol.*, 2016, **11**, 152.

129 C. Kural, H. Kim, S. Syed, G. Goshima, V. I. Gelfand and P. R. Selvin, *Science*, 2005, **308**, 1469–1472.

130 S. J. King and T. A. Schroer, *Nat. Cell Biol.*, 1999, **2**, 20–24.

131 J. Li, A. Johnson-Buck, Y. R. Yang, W. M. Shih, H. Yan and N. G. Walter, *Nat. Nanotechnol.*, 2018, **13**, 723–729.

132 T. E. Tomov, R. Tsukanov, Y. Glick, Y. Berger, M. Liber, D. Avrahami, D. Gerber and E. Nir, *ACS Nano*, 2017, **11**, 4002–4008.

133 X. Chen, C.-Y. Hong, Y.-H. Lin, J.-H. Chen, G.-N. Chen and H.-H. Yang, *Anal. Chem.*, 2012, **84**, 8277–8283.

134 Y. Chen, Q. Wang, J. Xu, Y. Xiang, R. Yuan and Y. Chai, *Chem. Commun.*, 2013, **49**, 2052–2054.

135 W. J. Wang, J. J. Li, K. Rui, P. P. Gai, J. R. Zhang and J. J. Zhu, *Anal. Chem.*, 2015, **87**, 3019–3026.

136 P. Miao, Y. Tang and J. Yin, *Chem. Commun.*, 2015, **51**, 15629–15632.

137 C. Yang, K. Shi, B. Dou, Y. Xiang, Y. Chai and R. Yuan, *ACS Appl. Mater. Interfaces*, 2015, **7**, 1188–1193.

138 X. Liu, Z. Yan, Y. Sun, J. Ren and X. Qu, *Chem. Commun.*, 2017, **53**, 6215–6218.

139 Y. Chang, M. Li, Z. Wu, Y. Zhuo, Y. Chai, Q. Xiao and R. Yuan, *Anal. Chem.*, 2018, **90**, 8241–8247.

140 S. Xie, Y. Dong, Y. Yuan, Y. Chai and R. Yuan, *Anal. Chem.*, 2016, **88**, 5218–5224.

141 Y. Zhao, H. Wang, W. Tang, S. Hu, N. Li and F. Liu, *Chem. Commun.*, 2015, **51**, 10660–10663.

142 Y. Zhao, S. Hu, H. Wang, K. Yu, Y. Guan, X. Liu, N. Li and F. Liu, *Anal. Chem.*, 2017, **89**, 6907–6914.

143 J. Zhu, H. Gan, J. Wu and H. Ju, *Anal. Chem.*, 2018, **90**, 5503–5508.

144 L. Zhu, Q. Liu, B. Yang, H. Ju and J. Lei, *Anal. Chem.*, 2018, **90**, 6357–6361.

145 C. B. Swearingen, D. P. Wernette, D. M. Cropek, Y. Lu, J. V. Sweedler and P. W. Bohn, *Anal. Chem.*, 2005, **77**, 442–448.

146 E. Chaloux and E. Altmann, Lead in Water: St. Paul Schools Delayed Fixes, http://www.kaaltv.com/article/stories/S4265242. shtml, (accessed March 13, 2019).

147 D. P. Wernette, C. Mead, P. W. Bohn and Y. Lu, *Langmuir*, 2007, **23**, 9513–9521.

148 B. Peeters, D. Daems, T. Van der Donck, F. Delport and J. Lammertyn, *ACS Appl. Mater. Interfaces*, 2019, **11**, 6759–6768.

149 M. H. S. Shyr, D. P. Wernette, P. Wiltzius, Y. Lu and P. V. Braun, *J. Am. Chem. Soc.*, 2008, **130**, 8234–8240.

150 A. J. Bonham, K. Hsieh, B. S. Ferguson, A. Vallée-Bélisle, F. Ricci, H. T. Soh and K. W. Plaxco, *J. Am. Chem. Soc.*, 2012, **134**, 3346–3348.

151 H. Li, N. Arroyo-Currás, D. Kang, F. Ricci and K. W. Plaxco, *J. Am. Chem. Soc.*, 2016, **138**, 15809–15812.

152 H. Li, P. Dauphin-Ducharme, G. Ortega and K. W. Plaxco, *J. Am. Chem. Soc.*, 2017, **139**, 11207–11213.

153 N. Arroyo-Currás, P. Dauphin-Ducharme, G. Ortega, K. L. Ploense, T. E. Kippin and K. W. Plaxco, *ACS Sens.*, 2018, **3**, 360–366.

154 W. Yan, L. Xu, C. Xu, W. Ma, H. Kuang, L. Wang and N. A. Kotov, *J. Am. Chem. Soc.*, 2012, **134**, 15114–15121.

155 S. Li, L. Xu, W. Ma, X. Wu, M. Sun, H. Kuang, L. Wang, N. A. Kotov and C. Xu, *J. Am. Chem. Soc.*, 2016, **138**, 306–312.

156 Y. Zhang, Z. Shuai, H. Zhou, Z. Luo, B. Liu, Y. Zhang, L. Zhang, S. Chen, J. Chao, L. Weng, Q. Fan, C. Fan, W. Huang and L. Wang, *J. Am. Chem. Soc.*, 2018, **140**, 3988–3993.

157 T. G. W. Edwardson, K. L. Lau, D. Bousmail, C. J. Serpell and H. F. Sleiman, *Nat. Chem.*, 2016, **8**, 162–170.

158 L. H. Reddy, J. L. Arias, J. Nicolas and P. Couvreur, *Chem. Rev.*, 2012, **112**, 5818–5878.

159 J. Li, C.-Y. Hong, S.-X. Wu, H. Liang, L.-P. Wang, G. Huang, X. Chen, H.-H. Yang, D. Shangguan and W. Tan, *J. Am. Chem. Soc.*, 2015, **137**, 11210–11213.

160 N. Li, J. Zheng, C. Li, X. Wang, X. Ji and Z. He, *Chem. Commun.*, 2017, **53**, 8486–8488.

161 X. Yang, Y. Wen, L. Wang, C. Zhou, Q. Li, L. Xu, L. Li, J. Shi, R. Lal, S. Ren, J. Li, N. Jia and G. Liu, *ACS Appl. Mater. Interfaces*, 2017, **9**, 38281–38287.

162 D. S. Seferos, D. A. Giljohann, H. D. Hill, A. E. Prigodich and C. A. Mirkin, *J. Am. Chem. Soc.*, 2007, **129**, 15477–15479.

163 T. L. Halo, K. M. McMahon, N. L. Angeloni, Y. Xu, W. Wang, A. B. Chinen, D. Malin, E. Strekalova, V. L. Cryns, C. Cheng, C. A. Mirkin and C. S. Thaxton, *Proc. Natl. Acad. Sci. U. S. A.*, 2014, **111**, 17104–17109.

164 A. E. Prigodich, P. S. Randeria, W. E. Briley, N. J. Kim, W. L. Daniel, D. A. Giljohann and C. A. Mirkin, *Anal. Chem.*, 2012, **84**, 2062–2066.

165 J. Pan, T.-G. Cha, F. Li, H. Chen, N. A. Bragg and J. H. Choi, *Sci. Adv.*, 2017, **3**, e1601600.

166 P. Zhang, C. Wang, J. Zhao, A. Xiao, Q. Shen, L. Li, J. Li, J. Zhang, Q. Min, J. Chen, H.-Y. Chen and J.-J. Zhu, *ACS Nano*, 2016, **10**, 3637–3647.

167 J. Chen, A. Zuehlke, B. Deng, H. Peng, X. Hou and H. Zhang, *Anal. Chem.*, 2017, **89**, 12888–12895.

168 H. Zhang, M. Lai, A. Zuehlke, H. Peng, X. F. Li and X. C. Le, *Angew. Chem., Int. Ed.*, 2015, **54**, 14326–14330.

169 X. Yang, Y. Tang, S. D. Mason, J. Chen and F. Li, *ACS Nano*, 2016, **10**, 2324–2330.

170 Y. Li, G. A. Wang, S. D. Mason, X. Yang, Z. Yu, Y. Tang and F. Li, *Chem. Sci.*, 2018, **9**, 6434–6439.

171 X. Qu, D. Zhu, G. Yao, S. Su, J. Chao, H. Liu, X. Zuo, L. Wang, J. Shi, L. Wang, W. Huang, H. Pei and C. Fan, *Angew. Chem., Int. Ed.*, 2017, **56**, 1855–1858.

172 C.-P. Liang, P.-Q. Ma, H. Liu, X. Guo, B.-C. Yin and B.-C. Ye, *Angew. Chem., Int. Ed.*, 2017, **129**, 9205–9209.

173 P.-Q. Ma, C.-P. Liang, H.-H. Zhang, B.-C. Yin and B.-C. Ye, *Chem. Sci.*, 2018, **9**, 3299–3304.

174 J. Wang, Q. Ma, Y. Wang, Z. Li, Z. Li and Q. Yuan, *Chem. Soc. Rev.*, 2018, **47**, 8766–8803.

175 R. C. Qian, L. Ding and H. X. Ju, *J. Am. Chem. Soc.*, 2014, **135**, 13282–13285.

176 E. Aznar, M. Oroval, L. Pascual, J. R. Murguía, R. Martínez-Máñez and F. Sancenón, *Chem. Rev.*, 2016, **116**, 561–718.

177 J. Wen, K. Yang, F. Liu, H. Li, Y. Xu and S. Sun, *Chem. Soc. Rev.*, 2017, **46**, 6024–6045.

178 X.-L. Li, N. Hao, H.-Y. Chen and J.-J. Xu, *Anal. Chem.*, 2014, **86**, 10239–10245.

179 F. Pu, Z. Liu, J. Ren and X. Qu, *Chem. Commun.*, 2013, **49**, 2305–2307.

180 P. Wu, K. Hwang, T. Lan and Y. Lu, *J. Am. Chem. Soc.*, 2013, **135**, 5254–5257.

181 W. Wang, R. Satyavolu Nitya Sai, Z. Wu, J. R. Zhang, J. J. Zhu and Y. Lu, *Angew. Chem., Int. Ed.*, 2017, **56**, 6798–6802.

182 M. Haase and H. Schäfer, *Angew. Chem., Int. Ed.*, 2011, **50**, 5808–5829.

183 S. Gai, C. Li, P. Yang and J. Lin, *Chem. Rev.*, 2014, **114**, 2343–2389.

184 Z. Yang, K. Y. Loh, Y.-T. Chu, R. Feng, N. S. R. Satyavolu, M. Xiong, S. M. Nakamata Huynh, K. Hwang, L. Li, H. Xing, X. Zhang, Y. R. Chemla, M. Gruebele and Y. Lu, *J. Am. Chem. Soc.*, 2018, **140**, 17656–17665.

185 J. Zhao, J. Gao, W. Xue, Z. Di, H. Xing, Y. Lu and L. Li, *J. Am. Chem. Soc.*, 2018, **140**, 578–581.

186 Z. Zhang, D. Balogh, F. Wang and I. Willner, *J. Am. Chem. Soc.*, 2013, **135**, 1934–1940.

187 Z. Zhang, F. Wang, D. Balogh and I. Willner, *J. Mater. Chem. B*, 2014, **2**, 4449–4455.

188 D. Balogh, M. A. Aleman Garcia, H. B. Albada and I. Willner, *Angew. Chem., Int. Ed.*, 2015, **54**, 11652–11656.

189 W.-H. Chen, X. Yu, A. Cecconello, Y. S. Sohn, R. Nechushtai and I. Willner, *Chem. Sci.*, 2017, **8**, 5769–5780.

190 W.-H. Chen, S. Yang Sung, M. Fadeev, A. Cecconello, R. Nechushtai and I. Willner, *Nanoscale*, 2018, **10**, 4650–4657.

191 W.-H. Chen, W.-C. Liao, Y. S. Sohn, M. Fadeev, A. Cecconello, R. Nechushtai and I. Willner, *Adv. Funct. Mater.*, 2018, **28**, 1705137.

192 C. E. Castro, F. Kilchherr, D.-N. Kim, E. L. Shiao, T. Wauer, P. Wortmann, M. Bathe and H. Dietz, *Nat. Methods*, 2011, **8**, 221–229.

193 G. Chatterjee, N. Dalchau, R. A. Muscat, A. Phillips and G. Seelig, *Nat. Nanotechnol.*, 2017, **12**, 920–927.

194 I. Mullor Ruiz, J.-M. Arbona, A. Lad, O. Mendoza, J.-P. Aimé and J. Elezgaray, *Nanoscale*, 2015, **7**, 12970–12978.

195 H. Chandran, N. Gopalkrishnan, A. Phillips and J. Reif, presented in part at the Proceedings of the 17th international conference on DNA computing and molecular programming, Pasadena, CA, 2011.

196 R. A. Muscat, K. Strauss, L. Ceze and G. Seelig, *ACM SIGARCH Comput. Archit. News*, 2013, **41**, 177–188.

197 M. Teichmann, E. Kopperger and F. C. Simmel, *ACS Nano*, 2014, **8**, 8487–8496.

198 H. Bui, S. Shah, R. Mokhtar, T. Song, S. Garg and J. Reif, *ACS Nano*, 2018, **12**, 1146–1155.

199 K. Lund, A. J. Manzo, N. Dabby, N. Michelotti, A. Johnson-Buck, J. Nangreave, S. Taylor, R. Pei, M. N. Stojanovic, N. G. Walter, E. Winfree and H. Yan, *Nature*, 2010, **465**, 206–210.

200 D. Wang, C. Vietz, T. Schröder, G. Acuna, B. Lalkens and P. Tinnefeld, *Nano Lett.*, 2017, **17**, 5368–5374.

201 E. Kopperger, T. Pirzer and F. C. Simmel, *Nano Lett.*, 2015, **15**, 2693–2699.

202 S. F. J. Wickham, M. Endo, Y. Katsuda, K. Hidaka, J. Bath, H. Sugiyama and A. J. Turberfield, *Nat. Nanotechnol.*, 2011, **6**, 166–169.

203 O. Mendoza, J.-L. Mergny, J.-P. Aimé and J. Elezgaray, *Nano Lett.*, 2016, **16**, 624–628.

204 Y. Yang, M. A. Goetzfried, K. Hidaka, M. You, W. Tan, H. Sugiyama and M. Endo, *Nano Lett.*, 2015, **15**, 6672–6676.

205 E. Kopperger, J. List, S. Madhira, F. Rothfischer, D. C. Lamb and F. C. Simmel, *Science*, 2018, **359**, 296–301.

206 J. Liu, L. Song, S. Liu, Q. Jiang, Q. Liu, N. Li, Z.-G. Wang and B. Ding, *Nano Lett.*, 2018, **18**, 3328–3334.

207 O. Idan and H. Hess, *Curr. Opin. Biotechnol.*, 2013, **24**, 606–611.

208 J. Fu, M. Liu, Y. Liu, N. W. Woodbury and H. Yan, *J. Am. Chem. Soc.*, 2012, **134**, 5516–5519.

209 J. Fu, Y. R. Yang, A. Johnson-Buck, M. Liu, Y. Liu, N. G. Walter, N. W. Woodbury and H. Yan, *Nat. Nanotechnol.*, 2014, **9**, 531–536.

210 C. Timm and C. M. Niemeyer, *Angew. Chem., Int. Ed.*, 2015, **54**, 6745–6750.

211 Y. Zhang, S. Tsitkov and H. Hess, *Nat. Commun.*, 2016, **7**, 13982.

212 C. Kielar, F. V. Reddavide, S. Tubbenhauer, M. Cui, X. Xu, G. Grundmeier, Y. Zhang and A. Keller, *Angew. Chem., Int. Ed.*, 2018, **57**, 14873–14877.

213 A. Shaw, I. T. Hoffecker, I. Smyrlaki, J. Rosa, A. Grevys, D. Bratlie, I. Sandlie, T. E. Michaelsen, J. T. Andersen and B. Högberg, *Nat. Nanotechnol.*, 2019, **14**, 184–190.

214 C. M. Erben, R. P. Goodman and A. J. Turberfield, *Angew. Chem., Int. Ed.*, 2006, **45**, 7414–7417.

215 A. Sprengel, P. Lill, P. Stegemann, K. Bravo-Rodriguez, E.-C. Schöneweiß, M. Merdanovic, D. Gudnason, M. Aznauryan, L. Gamrad, S. Barcikowski, E. Sanchez-Garcia, V. Birkedal, C. Gatsogiannis, M. Ehrmann and B. Saccà, *Nat. Commun.*, 2017, **8**, 14472.

216 A. Kuzyk, R. Jungmann, G. P. Acuna and N. Liu, *ACS Photonics*, 2018, **5**, 1151–1163.

217 B. Shen, M. A. Kostiainen and V. Linko, *Langmuir*, 2018, **34**, 14911–14920.

218 G. P. Acuna, F. M. Möller, P. Holzmeister, S. Beater, B. Lalkens and P. Tinnefeld, *Science*, 2012, **338**, 506–510.

219 A. Puchkova, C. Vietz, E. Pibiri, B. Wünsch, M. Sanz Paz, G. P. Acuna and P. Tinnefeld, *Nano Lett.*, 2015, **15**, 8354–8359.

220 S. E. Ochmann, C. Vietz, K. Trofymchuk, G. P. Acuna, B. Lalkens and P. Tinnefeld, *Anal. Chem.*, 2017, **89**, 13000–13007.

221 C. Heck, Y. Kanehira, J. Kneipp and I. Bald, *Angew. Chem., Int. Ed.*, 2018, **57**, 7444–7447.

222 A. Angelin, S. Weigel, R. Garrecht, R. Meyer, J. Bauer, R. K. Kumar, M. Hirtz and C. M. Niemeyer, *Angew. Chem., Int. Ed.*, 2015, **54**, 15813–15817.

223 D. Huang, K. Patel, S. Perez-Garrido, J. F. Marshall and M. Palma, *ACS Nano*, 2019, **13**, 728–736.

224 P. K. Dutta, Y. Zhang, A. T. Blanchard, C. Ge, M. Rushdi, K. Weiss, C. Zhu, Y. Ke and K. Salaita, *Nano Lett.*, 2018, **18**, 4803–4811.

225 M. D. Mager, V. LaPointe and M. M. Stevens, *Nat. Chem.*, 2011, **3**, 582–589.

226 F.-J. Lv, R. S. Tuan, K. M. C. Cheung and V. Y. L. Leung, *Stem Cells*, 2014, **32**, 1408–1419.

227 Z. Mitri, T. Constantine and R. O'Regan, *Chemother. Res. Pract.*, 2012, **2012**, 743193.

228 Y. Tang, Y. Lin, X. Yang, Z. Wang, X. C. Le and F. Li, *Anal. Chem.*, 2015, **87**, 8063–8066.

229 Y. S. Ang, J. E. J. Li, P.-J. Chua, C.-T. Ng, B.-H. Bay and L.-Y. L. Yung, *Anal. Chem.*, 2018, **90**, 6193–6198.

230 H. Liang, S. Chen, P. Li, L. Wang, J. Li, J. Li, H.-H. Yang and W. Tan, *J. Am. Chem. Soc.*, 2018, **140**, 4186–4190.

231 K. Ren, Y. Liu, J. Wu, Y. Zhang, J. Zhu, M. Yang and H. Ju, *Nat. Commun.*, 2016, **7**, 13580.

232 R. Peng, H. Wang, Y. Lyu, L. Xu, H. Liu, H. Kuai, Q. Liu and W. Tan, *J. Am. Chem. Soc.*, 2017, **139**, 12410–12413.

233 L. Qiu, T. Zhang, J. Jiang, C. Wu, G. Zhu, M. You, X. Chen, L. Zhang, C. Cui, R. Yu and W. Tan, *J. Am. Chem. Soc.*, 2014, **136**, 13090–13093.

234 K. Zhang, R. Deng, Y. Sun, L. Zhang and J. Li, *Chem. Sci.*, 2017, **8**, 7098–7105.

235 H. Li, M. Wang, T. Shi, S. Yang, J. Zhang, H.-H. Wang and Z. Nie, *Angew. Chem., Int. Ed.*, 2018, **130**, 10383–10387.

236 S. Artavanis-Tsakonas, M. D. Rand and R. J. Lake, *Science*, 1999, **284**, 770–776.

237 H. Bo, K. Fanpeng, G. Xiaonan, J. Lulu, L. Xiaofeng, G. Wen, X. Kehua and T. Bo, *Angew. Chem., Int. Ed.*, 2018, **130**, 5404–5407.

238 N. S. R. Satyavolu, K. Y. Loh, L. H. Tan and Y. Lu, *Small*, 2019, **15**, 1900975.

239 N. S. R. Satyavolu, N. Pishevaresfahani, L. H. Tan and Y. Lu, *Nano Res.*, 2018, **11**, 4549–4561.

240 N. S. R. Satyavolu, L. H. Tan and Y. Lu, *J. Am. Chem. Soc.*, 2016, **138**, 16542–16548.

241 L. H. Tan, Y. Yue, N. S. R. Satyavolu, A. S. Ali, Z. Wang, Y. Wu and Y. Lu, *J. Am. Chem. Soc.*, 2015, **137**, 14456–14464.

242 T. Song, L. Tang, L. H. Tan, X. Wang, N. S. R. Satyavolu, H. Xing, Z. Wang, J. Li, H. Liang and Y. Lu, *Angew. Chem., Int. Ed.*, 2015, **54**, 8114–8118.

243 Z. Wang, J. Zhang, J. M. Ekman, P. J. A. Kenis and Y. Lu, *Nano Lett.*, 2010, **10**, 1886–1891.

244 C. Carrillo-Carrión, R. Martínez, M. F. Navarro Poupard, B. Pelaz, E. Polo, A. Arenas-Vivo, A. Olgiati, P. Taboada, M. G. Soliman, Ú. Catalán, S. Fernández-Castillejo, R. Solà, W. J. Parak, P. Horcajada, R. A. Alvarez-Puebla and P. del Pino, *Angew. Chem., Int. Ed.*, 2019, **58**, 7078–7082.

245 C. Kielar, Y. Xin, B. Shen, M. A. Kostiainen, G. Grundmeier, V. Linko and A. Keller, *Angew. Chem., Int. Ed.*, 2018, **57**, 9470–9474.

246 N. Y. Wong, H. Xing, L. H. Tan and Y. Lu, *J. Am. Chem. Soc.*, 2013, **135**, 2931–2934.

247 J. Yang, Z. Meng, Q. Liu, Y. Shimada, R. C. L. Olsthoorn, H. P. Spaink, A. Herrmann and A. Kros, *Chem. Sci.*, 2018, **9**, 7271–7276.